Review Article

Ismeli Alfonso*, Federico González, Tania E. Soto, Joel Vargas, Claudio Aguilar, Ignacio A. Figueroa, and Gonzalo González

Analysis of the interactions between nonoxide reinforcements and Al–Si–Cu–Mg matrices

https://doi.org/10.1515/rams-2022-0271
received May 11, 2022; accepted September 21, 2022

Abstract: Nonoxide ceramics excel among the reinforcements used for aluminum matrix composites due to their variety of morphologies and mechanical properties. Among these reinforcements are carbides (SiC, B_4C, and WC); carbon materials (graphite, carbon fibers, carbon nanotubes, and graphene); nitrides (silicon nitride [Si_3N_4] and BN); and hollow Fe spheres. Although the effect of adding different percentages of reinforcements has been widely studied for Al matrices, matrix–reinforcement interactions need more attention. The consequences of these interactions can include interface formation, loss of alloying elements, reinforcement deterioration, modifications in the matrix microstructure, different precipitation sequences and kinetics, and interfacial diffusion of elements. These interactions may be significantly modified by the alloying elements, needing more in-depth analyses for a correct selection of the matrix–reinforcement system. Al matrices with Si, Cu, and Mg outstand, and the focus of the present work is their reciprocal interactions with nonoxide reinforcements. The novelty of this review consists of the analysis and discussion of these interactions, emphasizing the modifications originated by each one of these alloying elements, and the conditions needed to increase or avoid their effects on the composite. Besides, an analysis of the crystallography of the generated interfaces is presented, including their impact on mechanical properties. This could be helpful for a better understanding and selection of the matrix–reinforcement system, also serving as a benchmark study.

Keywords: Al alloys, Al–Si–Cu–Mg, reinforcement, composite, syntactic foam, interface

1 Introduction

As it is reported in different studies [1,2], the importance of the correct selection of the reinforcement–matrix system is essential in metal matrix composites (MMCs) due to different interactions, which may affect their mechanical properties. That is why it is important to analyze both the reinforcement and the alloy system, including alloying elements that could affect matrix and hence the composite material [3–8]. Among MMC, the use of aluminum matrix composites (AMCs) has considerably increased due to advantages such as elevated corrosion and tribological resistance, high strength-to-weight ratio, recyclability, and low cost [1–3]. The addition of reinforcements to Al alloys to form AMC widen the applications of these alloys, improving their properties. Some AMC components are brake rotors and pistons, rocker arms, drive shafts, energy storage flywheels, and sporting goods [1]. Although reinforcement is the dominant mechanism for their mechanical properties enhancement, aluminum alloys can be also strengthened by adding different alloying elements. The addition of Si, Cu, and/or Mg has revealed their functionality, highlighted due to the contribution of each one of them. Si provides excellent castability (high fluidity and low shrinkage); Mg strengthens the alloy, imparting good

* **Corresponding author: Ismeli Alfonso,** Instituto de Investigaciones en Materiales, Unidad Morelia, Universidad Nacional Autónoma de México, Campus Morelia UNAM, Antigua Carretera a Pátzcuaro 8701, Col. Ex-Hacienda de San José de la Huerta, C.P. 58190, Morelia, Michoacán, México, e-mail: ialfonso@unam.mx
Federico González: Departamento de Ingeniería de Procesos e Hidráulica, Universidad Autónoma Metropolitana-Iztapalapa, A.P. 55-534, 09340, Ciudad de México, México
Tania E. Soto, Joel Vargas: Instituto de Investigaciones en Materiales, Unidad Morelia, Universidad Nacional Autónoma de México, Campus Morelia UNAM, Antigua Carretera a Pátzcuaro 8701, Col. Ex-Hacienda de San José de la Huerta, C.P. 58190, Morelia, Michoacán, México
Claudio Aguilar: Department of Metallurgical and Materials Engineering, Universidad Técnica Federico Santa María, Av. España 1680, Casilla 110-V, Valparaíso, Chile
Ignacio A. Figueroa, Gonzalo González: Instituto de Investigaciones en Materiales, Universidad Nacional Autónoma de México, Circuito Exterior S/N, Cd. Universitaria, C.P. 04510, Ciudad de México, México

corrosion resistance; while Cu increases the strength and hardness of aluminum alloys, also improving machinability [3]. The presence of these elements leads to the formation of second phases such as Si, β-Mg_2Si, θ-Al_2Cu, S-Al_2CuMg, and Q-$Al_5Cu_2Mg_8Si_6$ [6–12]. Some of them are considered *in situ* reinforcements and components of an AMC [13–16].

Although the AMC can be manufactured using both solid and liquid state methods, there are significantly more interactions at temperatures higher than the melting point of the Al alloys [1]. That is why manufacturing processes involving casting Al alloys are more relevant than processes using wrought Al matrices. According to these, we are mainly focusing this review on liquid processing and casting Al alloys. These alloys are used in automotive and aerospace industries, motivated by their recyclability, excellent fluidity, medium strength, and low density [1]. Reinforcements added to these matrices can include a wide variety of ceramics, with shapes such as particles, discs, whiskers, rods, fibers, and tubes [17–25]. They present elevated Young's moduli (E), considerably increasing the mechanical properties of the Al alloys. AMC can be reinforced with oxide [26–32] or nonoxide reinforcements [33–51], both contributing with a considerable increase in the mechanical properties. Nonoxide reinforcements include carbides (SiC, B_4C, and WC) [33–40], nitrides (silicon nitride [Si_3N_4] and BN) [41,42], and carbon materials (carbon nanotube [CNT] [43–46], graphene [47–51], and graphite [20,51,52]). They have elevated elastic moduli (E) [3,52], which can reach 1,000 GPa for CNT [53]. E that represents the composite can significantly increase with the increment in the volumetric fraction of the reinforcement. The use of porous reinforcements has also increased, forming metal matrix syntactic foams (MMSFs). They are a kind of MMC, with a resistance higher than conventional foams and a low density [54–58]. The use Fe and SiC hollow spheres has excelled for MMSF reinforcement [57–61].

For both composites and syntactic foams, strengthening will depend not only on the kind and percentage of reinforcement but also on a strong bonding at the interface and other interactions. These reinforcements may react with molten Al alloys during the manufacturing process, forming different reaction products [62–65]. In this sense, crystallographic characteristics of the interfaces play an essential role [46,66,67].

A previous work [62] collected interfacial reactions and other interactions between oxide reinforcements and Al matrices including Si, Cu, and/or Mg as alloying elements. That recompilation showed the importance of analyzing each combination of alloy system–reinforcement. We decided to present this study as there are only a few studies on the interfacial reactions and other matrix–reinforcement interactions. Hence, we have included the interactions between these matrices and nonoxide reinforcements. We are expecting a wider variety of interactions when molten Al matrices come in contact with nonoxide reinforcements due to the differences in the chemical compositions of nonoxide compounds (not only Me_xO_y in the case of oxide reinforcements, where Me is a metal). Besides, we are including a more in-depth analysis of the crystallographic characteristics of the interfaces, which are essential for the strengthening degree of the composite. This topic has been less studied and needs more attention in future research. We extracted representative works from the literature for this review: 44 papers on SiC, 33 on B_4C, 16 on WC, 20 on Si_3N_4, 10 on BN, 42 on CNT, 4 on graphene, 9 on graphite, and 31 on Fe spheres. Nevertheless, few of these papers analyze the aforementioned interactions, the interfaces, and the formation of reaction products (24 papers on SiC, 11 on B_4C, 5 on WC, 8 on Si_3N_4, 6 on BN, 8 on CNT, 3 on graphene, 3 on graphite, and 11 on Fe hollow spheres). This shows that more research is necessary on these composites. Although in the last 20 years there is a large quantity of papers have been presented on AMC reinforced with nonoxides, this number significantly decreases if the search is reduced to Al matrices with Si, Cu, and/or Mg. This is shown in the graph in Figure 1a, which shows the number of papers that studied these matrices for each reinforcement (black bars). If these papers are analyzed in detail, there are only few works on the study of interfaces as mentioned earlier (see gray bars in Figure 1a). It is important to remark that this research topic has been increasing in this period for almost all the reinforcements, except for WC and BN, as it is shown in Figure 1b. This figure presents the number of papers on each reinforcement for periods of 5 years.

According to this search, this review could contribute to a better selection of nonoxide reinforcements depending on the alloying element content in the Al alloy. This article is organized as follows: Section 2 presents the nature of possible reinforcement–matrix interactions, followed by subsections that analyze these phenomena for each reinforcement when matrices are pure Al, followed by Al matrices with the addition of Si, Cu, and/or Mg.

2 Reinforcement–matrix interactions

Interfacial reactions and the possible formation of interfaces play a crucial role in the load transfer between the

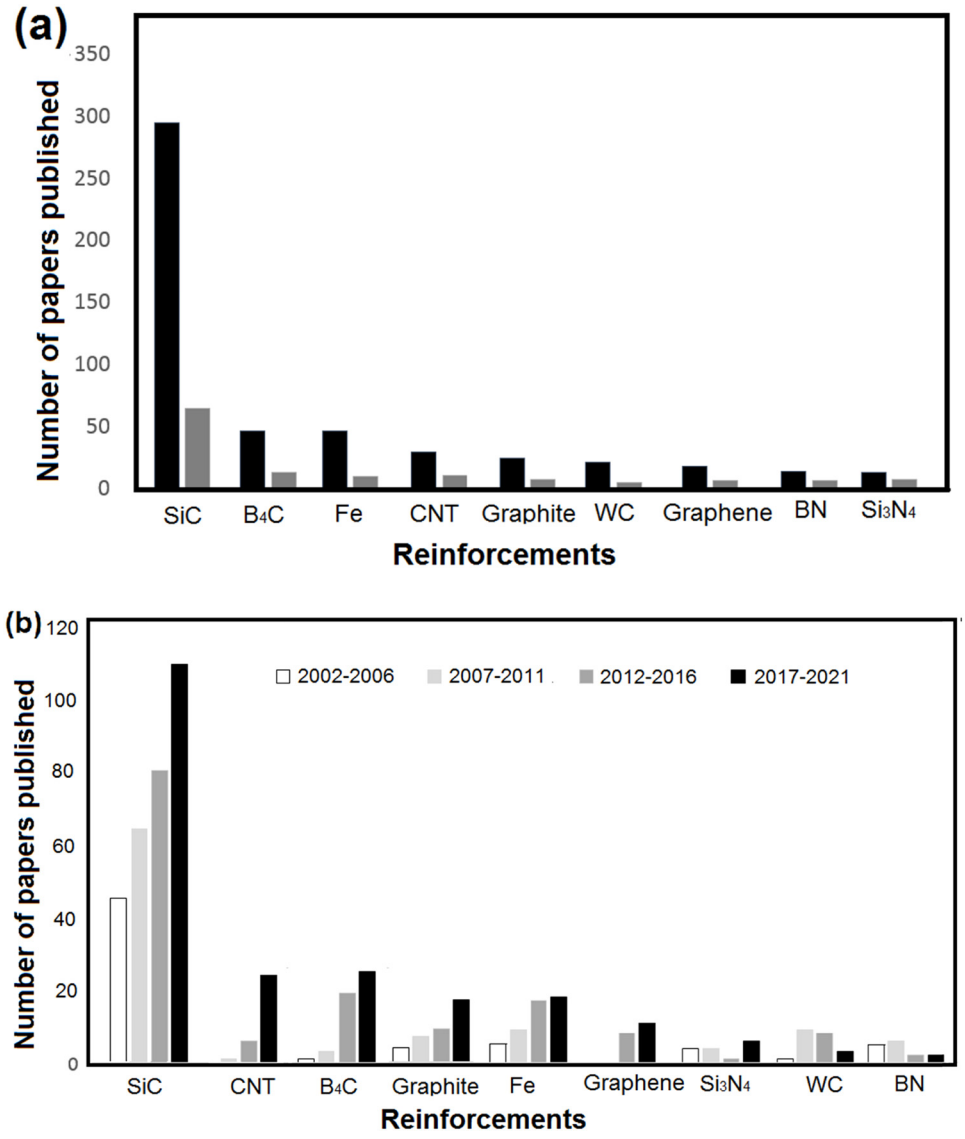

Figure 1: Number of papers published from 2002 to 2021: (a) on Al matrices with Si, Cu, and/or Mg reinforced with nonoxide reinforcements (black bars) and those papers that include the study of the interfaces (gray bars). (b) Number of papers published on this topic for periods of 5 years, from 2002 to 2021. Source: https://www.scopus.com.

matrix and the reinforcement. These phenomena depend on the compositions of the matrix and the reinforcement and on the manufacturing process, including variables such as time and temperature. The degree of strengthening depends on strong bonding at this interface, being desired interactions on the atomic or molecular levels. This is influenced by the crystallography of the interface and by the intermetallics formed in the interfacial region, including characteristics such as coherency or orientation relationship. The degree of wettability will influence these reactions and the interface characteristics, with or without interfacial layers of reaction products. If the interfacial products are brittle, the performance of the composite will be inadequate. In addition, interfacial reactions can deteriorate the reinforcement [65–67]. The bonding is governed by the nature of the interface, and its strength is linked to the wetting and the surface energy. The absence of interfacial bonding may be catastrophic for elastic and plastic behavior due to the total absence of load transfer. Besides, for fatigue behavior, a weak interface could favor cracking [68]. Although these interactions are more relevant for liquid-state manufacturing processes, they could also occur for solid-state processes [63,69–72].

One of the consequences of adding a reinforcement to a molten metal is the decrease in the volume fraction of

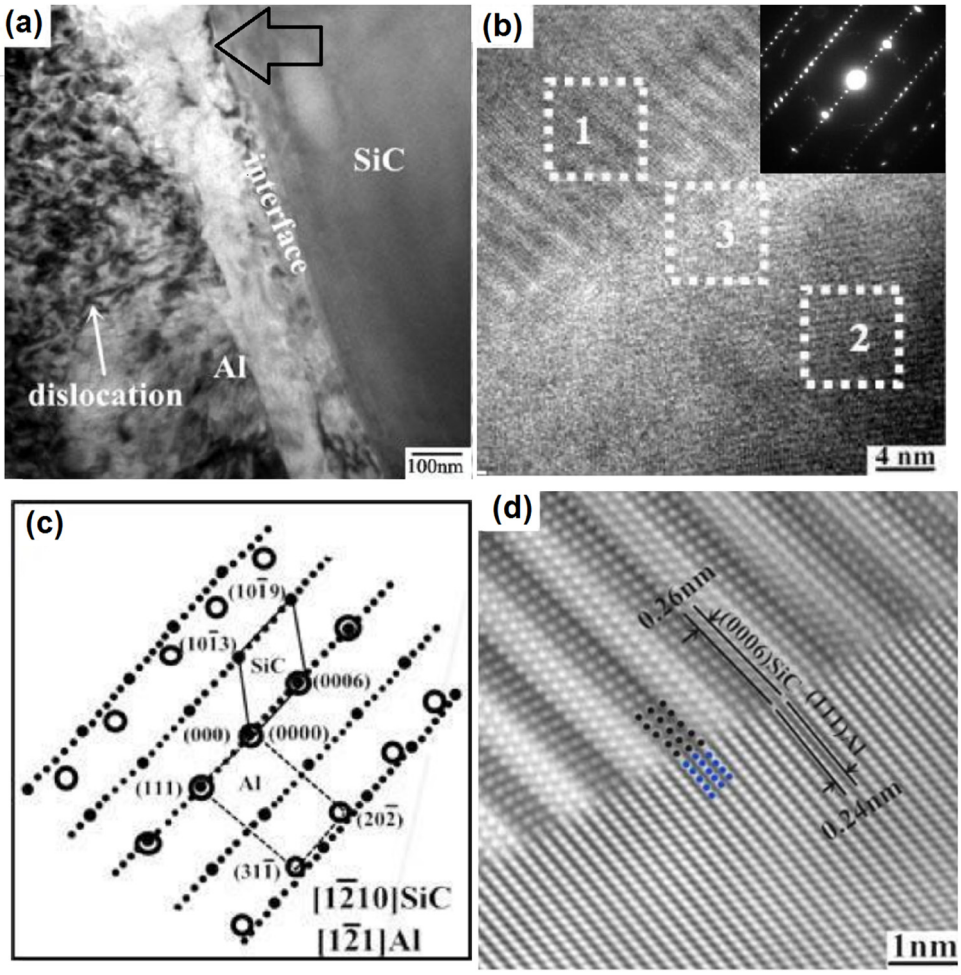

Figure 2: TEM (a) and HRTEM (b) images of the interface SiC/Al without interfacial products for an SiCp/Al–1.0Mg–0.6Si–0.25Cu composite, (c) indexed pattern of the SAED presented in Figure 2b, and (d) IFFT of the area 3 in Figure 2b (Reproduced with permission from [84].).

the molten alloy, from 100% to lower values while the volume fraction of the reinforcement increases. This can lead to a faster solidification compared to the solidification process for unreinforced alloys [1], reducing the latent heat, mainly when the molten matrix enters in contact with cooler reinforcements [72]. The solidification velocity for unreinforced alloys is mainly given by the mold, but the addition of reinforcements considerably increases nucleation centers [69,71,72]. A direct consequence of this process is the microstructure refinement [1].

Another consequence of the addition of reinforcements could be the modification of the precipitation process compared to unreinforced matrix alloys. These modifications include different precipitation kinetics, the formation of diverse types of precipitates, the absence of precipitates, and the precipitation in nonheat treatable alloys [73]. Although matrix hardening does not significantly influence stiffness of the AMC, it can improve yielding behavior and tensile properties [68].

In the following sections, these and other possible matrix–reinforcement interactions will be discussed for the most important nonoxide reinforcements used for Al matrices with the presence of Si, Cu, and/or Mg as alloying elements.

2.1 Silicon carbide (SiC)

SiC presents high hardness, stiffness, and elastic modulus (480 GPa); good shock behavior; elevated wear and erosion resistances; high thermal stability; and refractoriness. It can form a protective coating of silicon oxide, which leads to good oxidation properties [74–77]. SiC has been also used as hollow spheres for manufacturing syntactic foams [61]. The use of Al/SiC composites includes materials for nuclear plants, heat exchangers, optical devices, pistons, rotors, and brake discs [17].

2.1.1 SiC in Al matrices

SiC in contact with liquid Al is expressed through the following reaction [74,78–82]:

$$4\ Al_{(l)} + 3\ SiC_{(s)} = Al_4C_{3(s)} + 3\ Si_{(l)} \quad (1)$$

Salvo et al. [82] established that the extension of this reaction depends on both the alloy composition and the processing conditions, mainly temperature and time of contact between liquid metal and the reinforcement. Al_4C_3 obtained through this reaction is brittle and insoluble and is present as either isolated precipitates or continuous layers [83]. When the Al_4C_3 layer is not present, SiC is partially bonded to the matrix, and decohesion could occur at the interface, propagating and growing cracks. This is observed in the transmission electron microscopy (TEM) and Figure 2a–d shows images of a 6061 Al–1.0 Mg–0.6 Si–0.25 Cu alloy reinforced with SiC particles. Figure 2a shows a clean and smooth interface, without the formation of Al_4C_3 or other interfacial products [84]. Nevertheless, some decohesion seems to be present (arrowed) in this interface, which (i) limits load transfer and (ii) leads to crack propagation. It is a desired perfect and complete contact between SiC and Al, as shown in Figure 2b, which corresponds to a high-resolution TEM (HRTEM) image of the SiC/Al interface and its selected area electron diffraction (SAED) pattern. Figure 2c shows the indexed pattern, while Figure 2d shows the inverse fast Fourier transform (IFFT) obtained from area 3 in Figure 2b, with an orientation relationship (0006) SiC || (111) Al. Other reported orientation relationship is (10–10) SiC || (–111) Al) [85]. Such semi-coherent interfaces can effectively transfer the load from matrix to SiC. Nevertheless, the zones without effective bonding could provoke failures in the composite.

Otherwise, when the Al_4C_3 layer is present, the interfacial bond is stronger, and fracture propagates through the reinforcement instead of through the interface [83]. This makes a more efficient load transfer across the interface possible and leads to an increase in mechanical properties, although ductility decreases. Tham et al. [83] reported that values of ultimate tensile and yield strengths increased, respectively, 10 and 20% in composites with the presence of the Al_4C_3 layer, compared to composites without it. Nevertheless, if thickness of this interface is larger than a critical size, mechanical properties could be reduced. This can also occur when Al_4C_3 is obtained as isolated particles. Figure 3a and b shows an example of the formation of Al_4C_3 as a reaction product at the Al/SiC interface, for a 2009 Al alloy reinforced with 15 vol% SiC particles [86]. HRTEM in Figure 3b shows that the crystallographic orientation for Al_4C_3 corresponds to (–11 to 24) Al_4C_3 || (–101 to 6)SiC, without crystallographic orientation Al_4C_3/Al matrix. The composite obtained under these conditions presented excellent performance because SiC is completely bonded to the matrix, avoiding decohesion and improving load transfer, which raised the UTS. These authors also reported a crystallographic orientation (1–102)Al_4C_3 || (1–100)SiC. These different orientations depend on the nucleation conditions for Al on SiC and are focused to reduce the free energy of the interfaces. Aluminum has a face-centered cubic (fcc) lattice, with a = 0.405 nm. Otherwise, SiC can be present as 6H α-SiC, which has a hexagonal structure, with lattice parameters such as a = 0.30807 nm and c = 1.51174 nm, or as β-SiC, with a cubic structure (a = 0.43581 nm) [87]. On the other hand, Al_4C_3 crystallizes in the hexagonal unit cell, with crystallographic parameters a = 0.333 nm and c = 2.498 nm [88]. These characteristics make possible different orientation relationships for hexagonal SiC and Al_4C_3, with small lattice

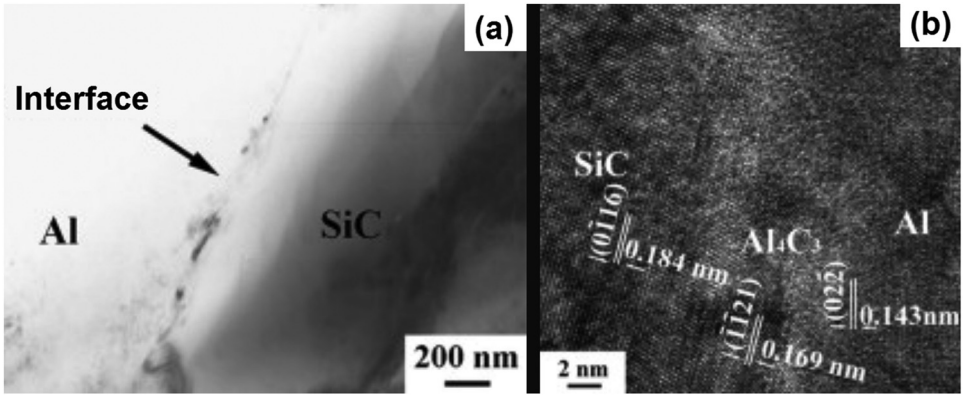

Figure 3: TEM (a) and HRTEM (b) images of the interface SiC/Al with the presence of the Al_4C_3 interlayer for a 2009 Al alloy reinforced with 15% SiC particles (Reproduced with permission from [86].).

mismatches. The Al_4C_3 reaction layer has the tendency to form semicoherent interfaces and orientation relationships with the aluminum matrix and the SiC particles [83]. Figures 2 and 3 show the effect that can exert not only the reinforcing type but also the addition of alloying elements on the crystallography of the interfaces. According to the matrix–reinforcement interaction, reaction products can be favored or avoided. These intermetallics commonly grows through mechanisms involving diffusion of elements from the reinforcement to the matrix and vice versa, presenting planes with the same crystallographic orientations. These interlayers increase the strength of the composites due to their strong bonding.

The occurrence of severe interfacial reactions can be detected not only by TEM but also by using optical microscopy (OM) or scanning electron microscopy (SEM), with ledges and pits at the interfaces, as showed in the study by Sritharan et al. [89]. This is shown in Figure 4a and b for an A359 aluminum casting alloy (9.27 Si and 0.55 Mg, in wt%) reinforced with 20 vol% of SiC particles. Differences in the SiC particles are observed for this composite before (Figure 4a) and after (Figure 4b) melting and held at 650°C for 48 h.

Because of the oxidation of SiC, the formation of SiO_2 occurs according to [90,91]:

$$SiC_{(s)} + 2O_{2(g)} = SiO_{2(s)} + CO_{2(g)} \quad (2)$$

The thickness of the SiO_2 layer is related to temperature: higher temperature increases layer thickness due to a higher diffusivity of oxygen, also improving wetting [91]. Its formation can modify the reaction to form Al_4C_3 because SiO_2 acts as a barrier and avoids further oxidation. Amorphous SiO_2 layers cover SiC, which acts as an intermediate to form stable interfaces and avoid Al_4C_3 formation [87]. The kinetics to obtain SiO_2 follows a linear-parabolic model, stabilizing the SiO_2 layer thickness when passive oxidation occurs [91]. After its formation, SiO_2 layer thickness could decrease through a reaction with molten Al, obtaining Al_2O_3 that reinforces the composite [92–95]. This reaction is expressed as follows:

$$3\,SiO_{2(s)} + 4\,Al_{(l)} = 2\,Al_2O_{3(s)} + 3\,Si_{(s)} \quad (3)$$

2.1.2 SiC in Al matrices with Si

The addition of Si to an Al alloy creates an equilibrium among SiC, Al_4C_3, and liquid Al, which is the possible modification of equation (1) due to the differences in the liquid composition [96,97]:

$$Si + x\,A1 = \{Si{-}A1_x\} \quad (4)$$

This can diminish or even avoid the formation of Al_4C_3 at the interface [96]. The required Si content in the matrix to prevent it increases with the increase in the melting temperature [78]. Schwabe et al. [97] found that at 750°C, this content was 6 at%, while at 1,300°C, the content was 16 at%. As shown in Figure 2a–d, Wang et al. [85] obtained a clean surface, without interfacial reactants, using an Al alloy with 19.5% Si to avoid Al_4C_3 formation. The dependence between Si content and temperature for the formation of Al_4C_3 was graphically presented in the study by Salvo et al. [82]. This study could be consulted for establishing manufacturing conditions according to the Si content.

2.1.3 SiC in Al matrices with Mg

It has been reported that the addition of Mg to Al alloys reinforced with SiC modifies equation (1), where Al_4C_3 formation is now accompanied with the formation of

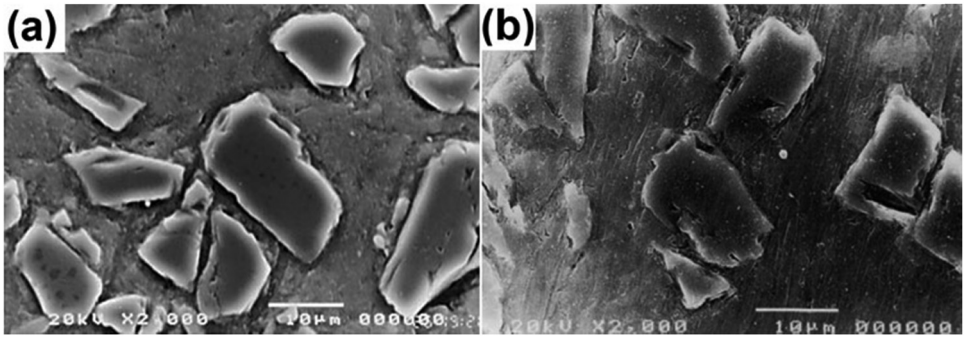

Figure 4: SEM images of an A359 + 20 vol% SiC particles AMC. (a) Before elevated temperature exposure, with SiC particles presenting relatively flat surfaces and interfaces. (b) After being held at 650 C for 48 h, with SiC surfaces presenting pits and ledges (Reproduced with permission from [89].).

Mg_2Si [79–81]. This can occur according to equations (5) and (6) [79–81,68]:

$$4\ Al_{(l)} + 3\ SiC_{(s)} + 6\ Mg_{(l)} = Al_4C_{3(s)} + 3\ Mg_2Si_{(s)} \quad (5)$$

$$SiC_{(s)} + 2\ Mg_{(l)} = Mg_2Si_{(s)} + C_{(l)} \quad (6)$$

Due to the formation of SiO_2 through the oxidation of SiC (according to equation (2)), the following reactions have been reported when Mg is added to Al matrices [94,95]:

$$4Mg_{(l)} + SiO_2(s) = Mg_2Si_{(s)} + 2MgO_{(s)} \quad (7)$$

$$SiO_2(s) + 2Mg_{(l)} = 2MgO_{(s)} + Si_{(s)} \quad (8)$$

These reactions show that Mg improves wetting between Al and SiC particles [93,98,99]. Mahendra et al. [100] reported that the addition of 1.5 wt% of Mg to a pure Al matrix was enough for improving wetting, obtaining better distribution of this reinforcement, and enhancing the mechanical properties.

Another effect of the addition of Mg is the formation of not only MgO but also spinel $MgAl_2O_4$, as reported by Gonzalez et al. [101]. The bonding strength between spinel phase and Al matrix is more than the double of the strength for the bond Al/Al_4C_3 [99]. Crystallographic studies using TEM and electron probe micro analysis demonstrated that transformation from MgO to $MgAl_2O_4$ is associated with a volume reduction of 11%. This led to an incomplete coverage of the SiC particles, which presented degradation. These interfacial layers were discontinuous, with $MgAl_2O_4$ crystals significantly bigger than the MgO ones [101]. MgO formation is favored for higher Mg contents at the SiC/Al interface, while $MgAl_2O_4$ is more stable for low Mg contents. Li et al. [102] found that spinel improved the bonding strength of the interface through the change of the fracture mechanism from pull-out (when MgO was at the interface) to tensile loading induced. In addition, Gonzalez et al. [101] found that the addition of Mg made the alloy age hardenable due to the rejection of combination with Si as a consequence of Al_4C_3 formation at the interface (equations (5)–(7)). The following reactions to obtain spinel $MgAl_2O_4$ can occur [94,103–105]:

$$2SiO_2(s) + 2Al_{(l)} + Mg_{(l)} = MgAl_2O_{4(s)} + 2Si_{(s)} \quad (9)$$

$$2Al_{(l)} + Mg_{(l)} + 2O_{2(g)} = MgAl_2O_{4(s)} \quad (10)$$

$$3Mg_{(l)} + 4Al_2O_3(s) = 3MgAl_2O_{4(s)} + 2Al_{(l)} \quad (11)$$

$$3SiO_2(s) + 4Al_{(l)} + 2MgO_{(s)} = 2MgAl_2O_{4(s)} + 3Si_{(s)} \quad (12)$$

$MgAl_2O_4$ can decompose after its formation, according to [101–104]:

$$MgAl_2O_{4(s)} + 3Mg_{(l)} = 4MgO_{(s)} + 2Al_{(l)} \quad (13)$$

2.1.4 SiC in Al matrices with Si and Mg

The addition of Si and Mg as alloying elements could lead to different modifications as the effect of Si stops Al_4C_3 formation and Mg reduces SiO_2 and forms Mg_2Si. As for the case of Al–Mg alloys, in the case of Al–Mg–Si system, there is the formation of MgO and $MgAl_2O_4$. This could modify Si and/or Mg quantities reported as optima for improving mechanical properties of the matrix. Sritharan et al. [106] found that matrices for optimum strengthening when SiC is used as reinforcement were Al–Mg and Al–Mg–Si with high Mg content (alloys 5XXX and 6XXX, with Mg contents from 0.5 to 5.5 wt%), and this is due to the formation of Mg_2Si precipitates. An example of the formation of beneficial interfacial layers in Al alloys with Si and Mg can be found in the study by Gao et al. [107]. These authors reported a continuous and well-bonded coherent $SiC/MgAl_2O_4/Al$ interface, without any gaps, which is beneficial for load transfer and strength improvement. This interface of ~10 nm can be observed in the TEM images of Figure 5a and b, where the HRTEM image of Figure 5b shows the coherency for the interfacial bond $SiC/MgAl_2O_4$ [107]. As mentioned earlier, the formation of MgO or $MgAl_2O_4$ as reaction layers depends on the alloying element content. For Al–Si–Mg alloys, the combination of Mg and Si to precipitate as Mg_2Si decreased the quantity of Mg, leading to obtain $MgAl_2O_4$ instead of MgO. This can be seen in the HRTEM images of Figure 5c and d for Al–Mg–Si/SiC composites, where MgO and $MgAl_2O_4$ interfaces look clean, indicating a good wetting and bonding [102]. MgO (of about 10 nm) was formed for a supersaturated solid solution, where the content of Mg in solution is high, while $MgAl_2O_4$ (50–100 nm) formation was for a matrix with Mg_2Si precipitates, which led to decrease in the content of Mg in the solid solution. This demonstrates the effect that can exert the reinforcement on the matrix and both matrix and reinforcement on the interfacial layer. Contrarily, Tekmen and Cocen [73] found the modification of the precipitation process due to the addition of SiC. They reported that for Al–Mg–Si matrices reinforced with SiC particles, the hardness peak was obtained at lower duration than that for the matrix alloy. The increase in the SiC content also led to obtaining higher hardness. These authors found that for a composite with 20 vol% SiC, the increase in Mg and Si amounts led to obtaining higher hardening [73]. This demonstrates that both the alloying element content and the reinforcement volume fraction influence matrix precipitation. A good bonding achieved at the $SiC/MgAl_2O_4$ interface with semicoherency has been reported by Luo [87], with four types of orientation relationships, which was favorable to the composite

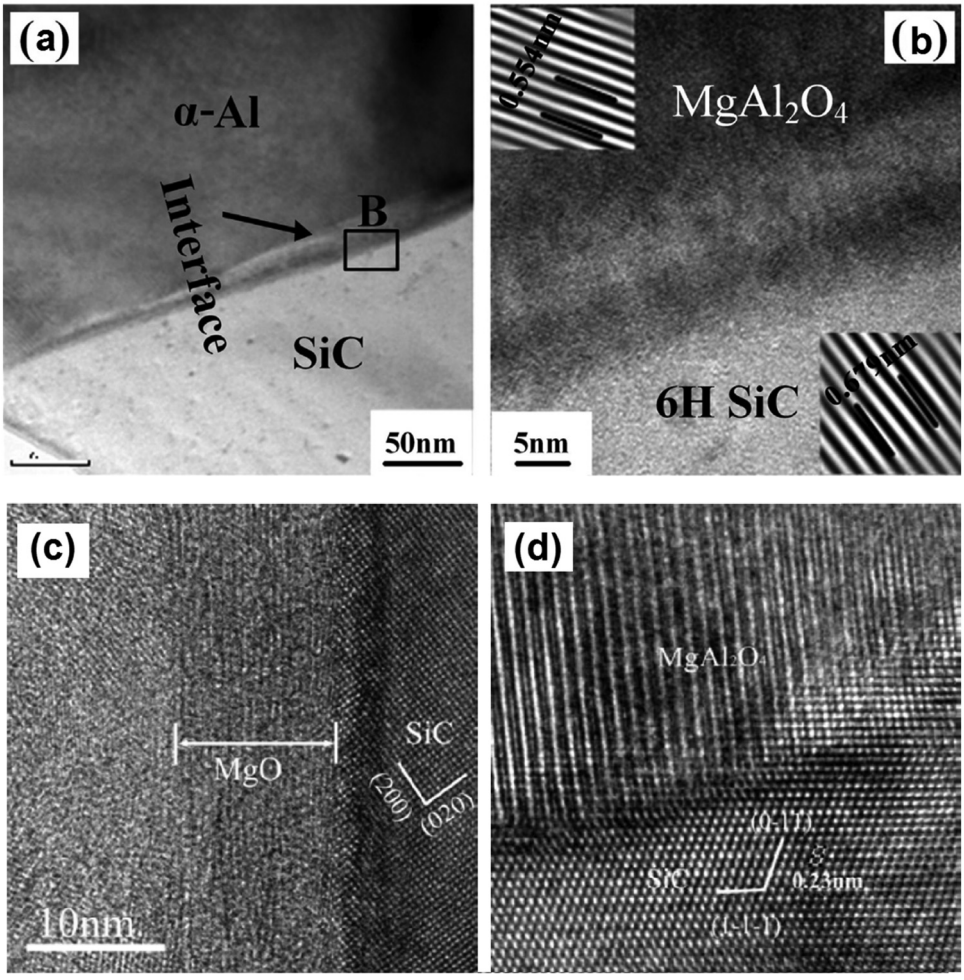

Figure 5: TEM images for pre-oxidized SiCp/Al–Cu–Mg-Si-Mn composites showing: (a) the SiC/$MgAl_2O_4$/Al interface and (b) HRTEM of the interface (area B in subsection b) (Reproduced with permission from [107].) (c and d) HRTEM of the interfaces obtained for Al–Mg–Si/SiC composites after a solution heat treatment (c), where MgO is obtained and overaged, (d) where $MgAl_2O_4$ can be observed (Reproduced with permission from [102].).

mechanical properties. Spinel $MgAl_2O_4$ has a face-centered cubic structure with a lattice parameter a = 0.8075 nm, while MgO is also fcc, with a = 0.421 nm [87]. These authors reported that due to the cubic cell, MgO may present the same orientation relationship of the spinel phase with SiC. The lattice mismatch Al/$MgAl_2O_4$ is 0.0028 (by counting 1/2 for the spinel phase), also presenting local structural rearrangements to achieve some degree of semicoherency at their interface.

Ren et al. [98] studied the combined effect of Si and Mg for Al alloys with different contents of Si (6, 12, and 18 wt%) and Mg (4, 8, and 12%), obtaining by infiltration composites reinforced with 55% of SiC particles. They found that Si contents less than 6% led to poor wettability and high porosity, not completely infiltrating SiC, while higher Si contents avoided the formation of Al_4C_3, and the composites presented higher elastic moduli, thermal dimensional stabilities, and thermal conductivities. Otherwise, the addition of Mg avoided the formation of Al oxides at the Al/SiC interface, lowering viscosity and surface tension [95]. The work of Sukumaran et al. [108] agrees with these results, demonstrating that both Si and Mg need to be added as alloying elements for obtaining good wettability SiC matrix, with concomitant effects essential to obtain composites with improved mechanical properties. Research including matrices combining these elements is insufficient and needs more attention.

2.1.5 SiC in Al matrices with Cu

Related to the effect of Cu on SiC–Al matrix interactions, Feng et al. [109] coated SiC particles with Cu using electroless plating, depositing a layer of Cu via dipping. They

found a supersaturated solid solution containing 37 wt% of Cu surrounding SiC, which strengthened the composite due to the lattice distortion. Another consequence of this coating was the precipitation of Al_2Cu around the SiC particles, hindering the dislocation movement and strengthening the composite. The presence of Cu additionally improved mechanical properties by increasing the interfacial bonding SiC–Al matrix, modifying it from SiC/Al to SiC/Cu and Cu–Al. This allowed a better load transfer from the Al matrix to the reinforcement [110]. These results show the effect of Cu improving mechanical properties through different mechanisms, which are examples of how a composite can present higher mechanical properties not only due to the addition of reinforcement but also due to other interactions matrix/reinforcement.

2.1.6 SiC in Al–Si–Cu–Mg matrices

The addition of more than two alloying elements to Al matrices contributes to stimulate interactions in the composites. An et al. [36] found that for these alloys Si reduced the interfacial free energy, improving the wettability of SiC. The content of this element was higher in the interfacial zone, diminishing the formation of Al_4C_3. The enrichment of the interface was not detected for Cu or Mg additions. Besides, Cu originated a slight deterioration of the wettability, also decreasing the formation of Al_4C_3. Moreover, Mg favored the wettability disrupting the oxide film covering Al [36]. For the combined study of these three elements, Durbadal and Srinath [111] found a thick reaction layer for a 2,124 Al–4.4 Cu–1.5 Mg–0.8 Si alloy reinforced with 10 wt% SiC. The interfacial products obtained when this alloy was re-melted at 900°C were associated with a high concentration of Cu, Mg, Si, and C, reporting the reaction of Al + SiC to form Al_4C_3 and Si. This indicated that SiC was dissociated, while Mg participated in the formation of spinel $MgAl_2O_4$.

Related to the effect of the reinforcement on the precipitation process for these alloys, Song et al. [112] found that for a 2,024 Al–4 Cu–1.5 Mg–0.5 Si alloy the amount of S′(Al_2CuMg) precipitates decreased due to the addition of SiC. This behavior is observed in Figure 6a–d. For the unreinforced alloy, an extensive precipitation was obtained, as shown in Figure 6a, while Figure 6b and c show that precipitation considerably decreased with the increase in the SiC content from 5 to 15 wt%, even presenting precipitation free zones in Figure 6d [112]. These modifications have a significant effect on the mechanical properties of the composites.

Examples as shown in Figure 6a–d and the explanations of these behavior were explained earlier for binary and ternary alloy systems reinforced with SiC. Independently of the alloying elements, the addition of reinforcements may lead to modify precipitation sequences and kinetics. Other precipitates have been observed in the interfacial region for this alloy system reinforced with SiC, as demonstrated in the study by Gatea et al. [113]. They found Al_2Cu, $Al_4Cu_2Mg_8Si_7$, and $MgAl_2$ at the SiC/Al alloy interface for an Al–1 Cu–1.2 Mg–0.8 Si alloy reinforced with SiC particles. On the other hand, for an Al–3.8 Cu–1.2 Mg–0.25 Si alloy, Guo et al. [114] observed that Mg was preferentially localized close to the SiC/matrix interfaces due to the formation of Mg_2Si. This led to the increase of the matrix hardness near the reinforcements. Pal et al. [110] reported that for an Al–5.4 Cu–1.5 Mg–0.3 Si alloy reinforced with SiC particles, the aging kinetic for the matrix was slower compared to the unreinforced alloy. This behavior was attributed to the segregation of alloying elements from the matrix to the interface. The decrease of Cu and Mg contents in the matrix reduced solute supersaturation, leading to this modification of the precipitation kinetic [110,115,116]. The nucleation of precipitates such as Al_2Cu can occur in the presence of Si, released by the interfacial reactions. Si–vacancies pairs favor homogeneous nucleation through the formation of dislocation loops [68]. Varma et al. [115] reported that the size of the reinforcement also affects precipitation hardening. They found that the use of particles of ~1 μm in diameter led to a higher precipitation hardening at a lower time compared to composites containing coarser reinforcements, which was attributed to faster diffusion of the alloying elements in Al.

Other properties could be also affected depending on the alloying elements content. For example, Wang et al. [117] found that the wear resistance of AMC with Al–Cu, Al–Mg, and Al–Si alloy matrices reinforced with SiC fibers decreased in that specific order, although hardness behavior of the matrices was inverse (48 HV for Al–Cu, 57 HV for Al–Mg, and 67 HV for Al–Si). This was attributed to the effect of interfacial reactions between fibers and matrices, not depending on the matrices hardness: a smooth Al_4C_3 coherent interface for Al–Cu; a nonsmooth interface, enough to increase both the interfacial bonding strength and wear resistance for Al–Mg; and no interfacial reactions for the composite with Al–Si matrix, presenting the lowest wear resistance between these composites. These results show that the formation of an interfacial bond particle–matrix is essential for increasing the wear resistance of these composites.

After the analysis of the interactions between SiC and Al matrices with Si, Cu, and/or Mg, it was found that the effect of each one of these elements is different. Adding Si

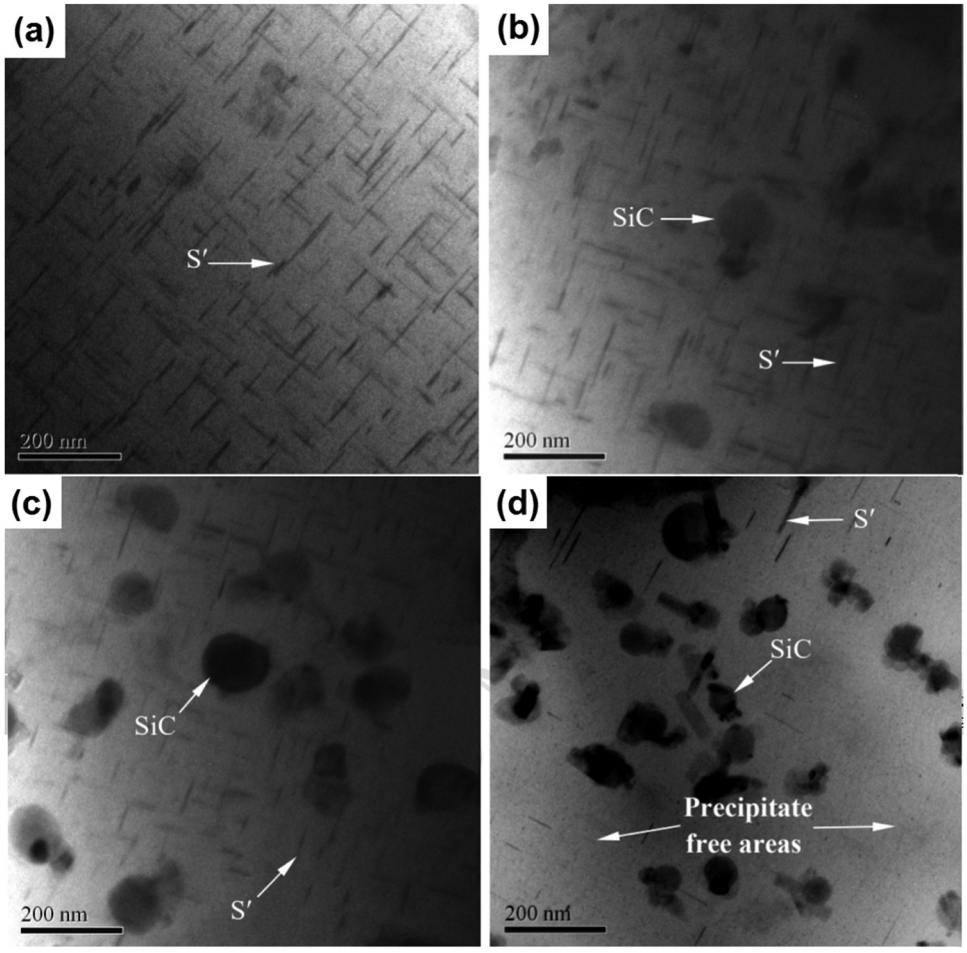

Figure 6: TEM images of a 2024 aluminum alloy reinforced with (a) 0, (b) 5 wt%, (c) 10 wt%, and (d) 15 wt% of SiC, after being initially aged at 110°C for 8 h, and then aged at 190°C for 24 h. S′ precipitates and SiC reinforcements can be observed (Reproduced with permission from [112].).

may lead to minimize or even avoid the reduction reaction of SiC with Al, lead to a higher elastic modulus, and decrease properties such as wear resistance, and this is due to low interfacial strength. On the other hand, Mg modifies wettability, but optima additions are not well specified or did not coincide in the literature. This element forms different interfacial compounds due to its interaction with SiC. Finally, interfacial compounds were not found when Cu was added to Al matrices apart from the characteristic precipitates obtained according to the matrix composition.

2.2 Tungsten carbide (WC)

WC is an attractive reinforcement for AMC due to its high melting point (2,780°C), hardness (2,242 HV), and elastic modulus (700 GPa), also presenting good wettability in Al [118,119]. It has elevated wear and abrasion resistances, high rigidity, impact resistance, and thermal conductivity; and can be used to reinforce Al alloys in applications such as machining tools, ammunitions, and surgical instruments [17].

2.2.1 WC in Al matrices with Si, Cu, and/or Mg

According to Sharath Kumar et al. [39], WC offers strong bonding with aluminum. These authors did not find any interfacial product for the reinforcement of an Al–5 Si–3 Cu–0.5 Mn alloy adding 7.5 wt% of WC to the molten alloy at 800°C. Nevertheless, it is reported that at higher temperatures the reaction between Al and WC particles could lead to the formation of $Al_{12}W$ and Al_4C_3, in addition to the eutectic structure of the Al–12 Si alloy [120]. For an Al–2.5 Mg–1.6 Cu–1.5 Zn–0.5 Fe–0.4 Si alloy reinforced with WC using stir casting, the formation of Al_5W

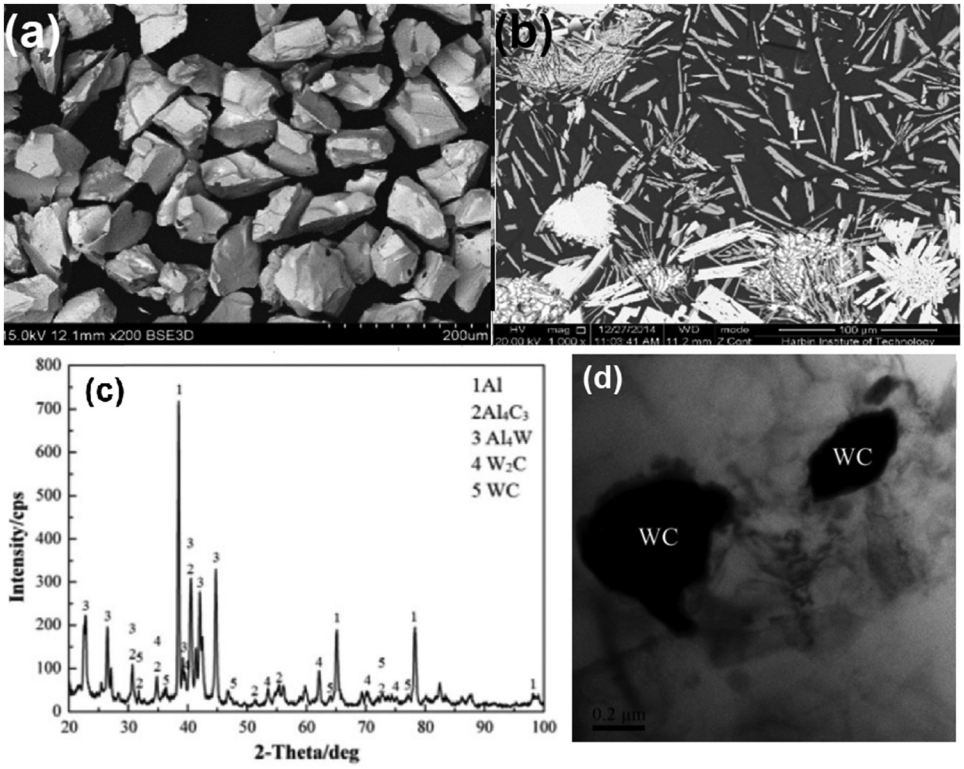

Figure 7: SEM images of (a) WC particles used as reinforcement and (b) the composite obtained after adding the WC particles to a 6061 Al alloy (0.8–1.2 Mg, 0.40–0.8 Si, 0.7max.Fe, 0.15–0.40 Cu), using laser welding. (c) XRD diffractogram of the obtained WC/Al composite. (Reproduced with permission from [123].) (d) TEM image of an Al/3vol%WC composite (Reproduced with permission from [128].).

was found, needing a more in-depth analysis of the interface [121]. Zhang et al. [122] reported that intermetallics such as Al_5W and $Al_{12}W$ can improve properties including mechanical strength, oxidation resistance, and thermal stability. Otherwise, Lekatou et al. [38] reported the formation of $Al_{12}W$ as coarse polygonal particles and Al_5W acicular plates for an Al1050 alloy reinforced with 1 vol% of WC processed at 830°C. These authors also reported the formation of Al_4C_3 through the following reactions depending on the contact temperature:

At 830°C:

$$19Al_{(l)} + 3WC_{(s)} = 3Al_5W_{(s)} + Al_4C_{3(s)} \quad (14)$$

On cooling at 697°C:

$$7Al_{(l)} + Al_5W_{(s)} = Al_{12}W_{(s)} \quad (15)$$

On cooling at 661°C:

$$Al_{(l)} + Al_{12}W_{(s)} = 13Al_{(\text{solid solution, peritectic})} \quad (16)$$

The presence of intermetallic particles (e.g., $Al_{12}W$) may reduce plastic deformation in the matrix due to crack growth mechanisms. The use of techniques implying elevated temperatures leads to the formation of different interfacial products, which could be detrimental to the compactness behavior of the MMC, as reported by Li et al. [123]. They reinforced a 6061Al alloy (0.8–1.2Mg, 0.40–0.8Si, 0.15–0.40Cu) with an Al–11.52Si wire and WC powder using laser welding and found rod-like Al_4W, W_2C, and Al_4C_3. The consequences of this process are shown in Figure 7a and b, where there are observed irregular WC particles before laser welding (Figure 7a); the microstructure is obtained after the manufacturing process (Figure 7b), consisting of Al matrix and the aforementioned rod-like phases. The X-ray diffraction (XRD) diffractogram depicted in Figure 7c demonstrates the formation of these new phases. No interfacial products were detected for low-temperature manufacturing methods, although excellent interfacial bonding is reported [124,125], contrary to the observed for other reinforcements added by these methods where decohesion occurs (e.g., TiO_2 [126]). Nevertheless, Singh and Sharma [127] studied an Al–18.5 Si–1.6 Cu–1.1 Mg–0.5 Fe alloy reinforced with 3–12 wt% WC particles using stir casting, revealing that Al_5W and $Al_{12}W$ precipitated, but only after T6 heat treatment. Although this alloy has high alloying elements content, no other intermetallics were detected. An example of the strong bonding for WC/Al composites is the manufacturing

process for reinforcing Al with 3 vol% of WC particles through roll bonding at 250°C, where it was possible to obtain excellent WC particle distribution, without interfacial reactions [128]. A TEM image in Figure 7d shows this composite and WC particles with smooth and clean interfaces, without visible decohesion. This led to a composite with enhanced tensile, hardness, and wear properties, also attributed to a uniform distribution of the reinforcements and a strong interfacial bonding.

Other elevated temperature processes that reveal the formation of different intermetallics have been reported, as shown in the work of Prasad et al. [129], coating an Al356.2 alloy with WC-Co, which led to the formation of W_2C. This resulted in the loss of reinforcement, embrittling the matrix and decreasing the mechanical properties. Moreover, Staia et al. [130] studied the superficial modification of an Al–7.0 Si–0.3 Mg alloy reinforcing with WC particles by laser alloying and identified W_2C produced by the oxidation of WC. This led to the release of C into the matrix and to the formation of Al_4C_3. Laser processing and the subsequent solidification process led to the formation of $W_6C_{2.54}$ and WC_x due to the partial dissolution of WC in the melting pool. WC is one of the reinforcements, which need more attention and research, including the analysis of the possible reaction products. This is shown in Figure 1.

Although the earlier analyzed alloys are rich in Si, Cu, and/or Mg, information was not found related to the formation of other phases with their presence. This shows the inertness of WC and the possibilities of its use. Nevertheless, more research and in-depth analysis of the interfacial regions are needed to elucidate if these elements have any effect on the interfaces, such as wettability modification, segregation, or effects on the mechanical properties.

2.3 Boron carbide (B_4C)

B_4C is considered the third hardest material (hardness of 3,800 Hv,) next to diamond and boron nitride (BN). It has low specific density (2.52 g·cm^{-3}), high stiffness (445 GPa), high chemical resistance, and good nuclear properties [131]. It can be used in AMC in applications such as abrasives, nozzles, and ballistic armors [17].

2.3.1 B_4C in Al matrices

It is reported that when B_4C is in contact with molten Al above 1,000°C, the formation of boron oxide (B_2O_3) films occurs around B_4C, increasing its wettability [132,133]. $AlB_{40}C_4$, $Al_2B_{48}C_8$, $Al_2B_{51}C_8$, $Al_3B_{48}C_8$, $Al_8B_4C_7$, and $B_{12}(B,C,Al)_3$ have been reported as interfacial reaction products [131,134–136]. Below 1,000°C, wettability is poor, being added different compounds (e.g., K_2TiF_6) to the removal of the oxide film from the aluminum surface, which reactivates wetting [131,134,135]. Some reaction products formed at these lower temperatures include Al_3BC, AlB_2, $Al_2B_4C_4$, and $Al_3B_{48}C_2$. Al_3BC formation occurs as follows [137–142]:

$$3Al_{(l)} + B_4C_{(s)} = Al_3BC_{(s)} + 3B_{(l)} \quad (17)$$

If the temperature is increased to 1,200–1,400°C, the formation of Al_4C_3, $AlB_{24}C_4$, $Al_8B_4C_7$, and $AlB_{12}C_2$ can occur [141]. The main reaction for the formation of Al_4C_3 is as follows [142]:

$$3B_4C_{(s)} + 10Al_{(l)} = 6AlB_{2(s)} + Al_4C_{3(s)} \quad (18)$$

Although the extensive reaction between Al and B_4C occurs above 1,100°C, it has been reported that it can even start at temperatures as low as 450°C. At temperatures higher than 600°C, the depletion of the aluminum content in the composite begins due to the formation of Al_2B [143].

2.3.2 B_4C in Al matrices with Mg

The presence of Mg in Al matrices results in the formation of $Al_xMg_{(1-x)}B_2$, Al_4C_3, $Al_x(B–C–O)_{1-x}$, and MgB_6 [104]. This element significantly increases wetting due to its ability to form strong bonds between matrix and B_4C by producing layers of $(Al,Mg)B_2$ [137–139]. The formation of $Mg(Al)B_2$ was also reported by Zhou et al. [140], who found that the *in situ* formation of this reinforcement led to a higher strength. Initially, its formation started in equation (17) and then in the following equation [137–140]:

$$2B_{(l)} + Mg_{(l)} + Al_{(l)} = Mg(Al)B_{2(s)} \quad (19)$$

For Al-(2.5–4.5) wt% Mg reinforced with B_4C, fabricated by pressureless infiltration at 800°C, Lee et al. [144] found the formation of AlB_2, AlB_{12} ($Al_3B_{48}C_2$), AlB_{10} ($AlB_{24}C_4$), and Al_3BC. They also detected the presence of $MgAl_2O_4$, phase reported for composite systems such as Al/SiC, Al/Al_2O_3, Al/BN, and Al/Si_3N_4 [145–147]. Otherwise, Lucas et al. [142] reported that reaction products for an Al–7Si–0.35Mg alloy reinforced with B_4C were Al_4C_3, MgB_2, and $Al_xMg_{(1-x)}B_2$ (where $0 < x < 1$). These authors found a higher Mg concentration in the interfacial reaction zone of B_4C, compared to the same region when the reinforcement was SiC. The reaction Mg/B_4C for Mg alloys is as follows [148]:

$$2Mg_{(l)} + B_4C_{(s)} = 2MgB_{2(s)} + C_{(s)} \quad (20)$$

Similar to the formation of Al_4C_3 and Mg_2Si for the reaction of Al and Mg with SiC (in equation (5)), when B_4C is used as reinforcement, the following reaction occurs:

$$6Mg_{(l)} + 4Al_{(l)} + 3B_4C_{(s)} = 6MgB_{2(s)} + Al_4C_{3(s)} \quad (21)$$

The transformation of MgB_2 into $Al_xMg_{(1-x)}B_2$ can also occur due to the diffusion of Al atoms into MgB_2, substituting Mg atoms [149]. This phase, reported as $Al0_{0.29}Mg0_{0.71}B_2$ by Suárez et al. [149], increased the microhardness of these composites. The diffusion of Al to form this phase can be presented by the following transformation:

$$MgB_{2(s)} + 0.29\ Al_{(l)} = Al_{0.29}Mg_{0.71}B_{2(s)} + 0.29Mg_{(l)} \quad (22)$$

It can be more generally presented as follows:

$$MgB_{2(s)} + xAl_{(l)} = Al_xMg_{(1-x)}B_{2(s)} + xMg_{(l)} \quad (23)$$

2.3.3 B_4C in Al matrices with Si

When an Al molten alloy in contact with B_4C contains Si, the formation of Al_4C_3 can be avoided due to the reaction between Si (dissolved) and C (in B_4C) [33]. This originates a reduction of the carbon activity by depleting its content in the carbide phase and leads to the formation of SiC instead of Al_4C_3. The presence of SiC improves the mechanical properties of these composites. Frage et al. [33] found that the Si content threshold value (necessary for preventing the formation Al_4C_3) is about 12 wt%, then favoring the formation of SiC.

Different intermetallics have been reported for composites obtained through the infiltration of B_4C with liquid Al and Al alloys (13 and 40 wt% Si) at 1,100°C, followed by a heat treatment for 10 h at 1,200°C [35]. AlB_{12} was obtained after infiltration, and ternary compounds such as $AlB_{12}C_2$, $Al_8C_7B_4$, and $Al_4C_4B_x$ are obtained after heat treatment. Al_4C_3 was obtained for low Si contents, while SiC was favored when the Si content was high.

2.3.4 B_4C in Al–Si–Cu–Mg matrices

For quaternary matrices, such as those reported in the research of Li et al. [150] for an Al–1.0 Mg–0.65 Si–0.25 Cu alloy reinforced with 20 wt% of B_4C, some of the reaction products are Al_3BC, MgO, $MgAl_2O_4$, MgB_7, $Mg_{0.78}Al_{0.75}B_{14}$, $Al_{12}BC_2$, and Al_4SiC_4. These authors divided reactions involving Mg and Si into two series according to their interactions with B_4C: first, the reactions involving B and Mg, and once they ended, the reactions involving Al, Si, and C stars (at temperatures higher than 620°C). These reactions initiated with equation (17), including the reaction of equation (11) to form $MgAl_2O_4$ and the following reactions:

$$1/3Al_{(l)} + B_4C_{(s)} = 1/3AlB_{12}C_{2(s)} + 1/3\ C_{(s)} \quad (24)$$

$$2Mg_{(l)} + O_{2(g)} = 2MgO_{(s)} \quad (25)$$

$$3Mg_{(l)} + B_2O_{3(s)} = 3MgO_{(s)} + 2B_{(l)} \quad (26)$$

$$3Mg_{(l)} + Al_2O_{3(s)} = 3MgO_{(s)} + 2Al_{(l)} \quad (27)$$

$$Mg_{(l)} + 7B_{(l)} = MgB_{7(s)} \quad (28)$$

$$4Al_{(l)} + Si_{(l)} + 4C_{(s)} = Al_4SiC_{4(s)} \quad (29)$$

These reactions lead to severe depletion of Mg in the Al matrix, decreasing its precipitation hardening. The deterioration of B_4C also leads to a decrease in the mechanical properties. Xue et al. [151] found that for these alloys, the addition of B_4C inhibits the formation of Guinier Preston zones and changes the order of precipitation. With the increase of the B_4C volume fraction, time for reaching hardening-peak decreased, but its intensity increased. Zhou et al. [152] studied an Al–1.0 Mg–0.65 Si–0.25 Cu (wt%) matrix reinforced with 26 wt% B_4C and found Al_3BC nanoparticles at the interface, surrounded by a thin layer of Cu. This led to the absence of the typical Q ($Al_5Cu_2Mg_8Si_6$) precipitates in the zone near B_4C particles. Precipitates were MgB_2 instead of Q. Al_3BC and MgB_2 can be obtained through the reaction of equation (18), followed by:

$$2B_{(l)} + Mg_{(l)} = MgB_{2(s)} \quad (30)$$

Moreover, Lee et al. [144] found MgO and TiB_2 instead of AlB_2 and Al_3BC for an Al–0.529 Si–0.954 Mg–0.172 Cu alloy reinforced with B_4C, with good interfacial. Besides, they reported the diffusion of Al toward B_4C during the stir casting process, followed by the interfacial reaction to generate an Al_4C_3 layer. Pozdniakov et al. [153] studied an Al–5% Cu alloy reinforced with 2, 5, and 7 wt% of B_4C manufactured using squeeze casting and found that reactions alloy/B_4C only led to the formation of Al_3BC and AlB_2, which assured good wettability. No reactions between Cu and B_4C were found, which agrees with the aforementioned reports. These authors reported the acceleration of the Al_2Cu precipitation due to the addition of B_4C. Manning and Gurganus [154] also found the null effect for Cu. Its addition did not cause significant modifications on the contact angle between B_4C and the molten Al alloy. Nevertheless, for high contents of Mg and Si, this angle significantly decreased, leading to good wettability and homogeneous distribution of B_4C particles. An example of well-distributed B_4C particles is shown in Figure 8a for an Al–1.0 Mg–0.65

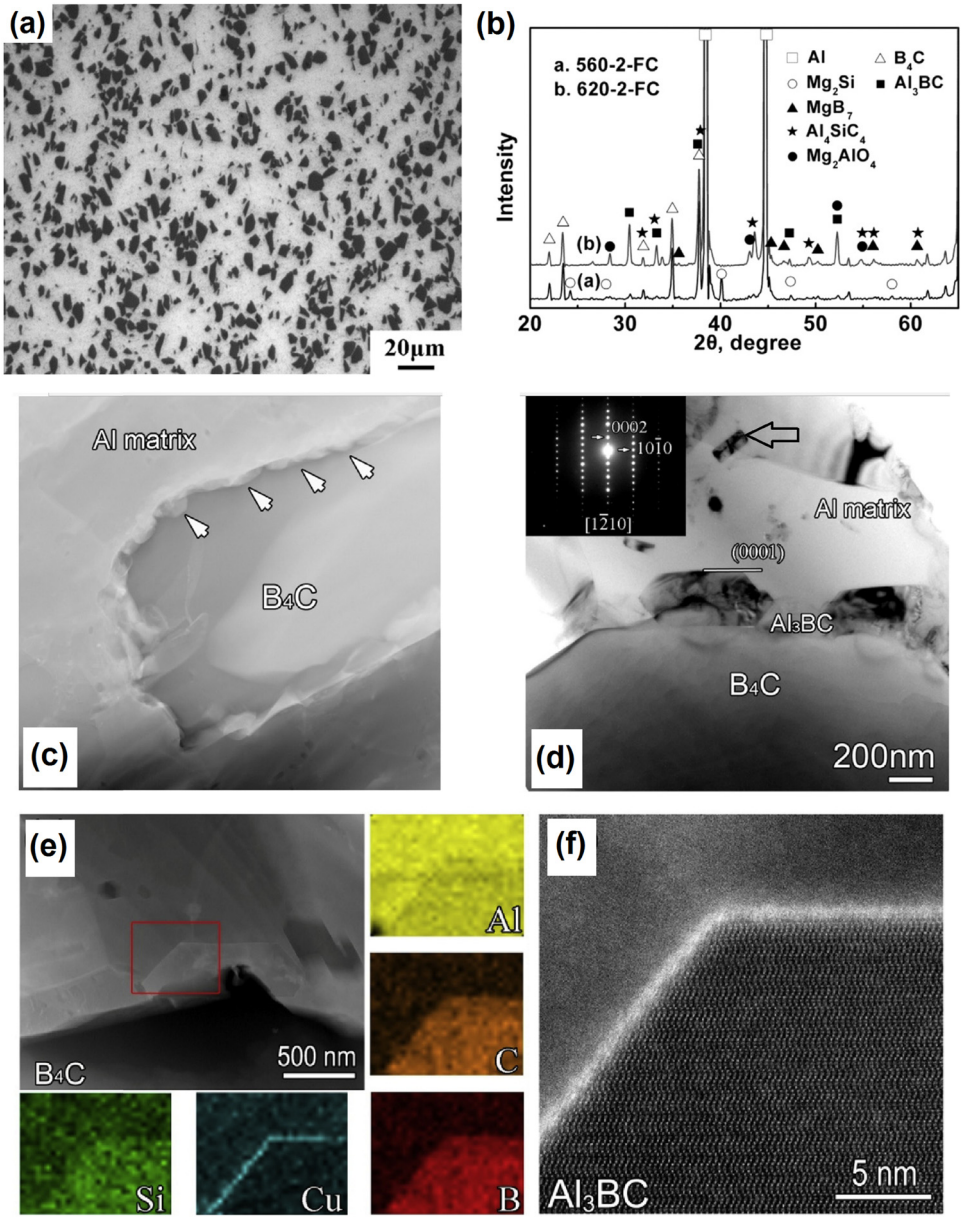

Figure 8: (a) OM image of an Al–1.0 Mg–0.65 Si–0.25 Cu (wt%) alloy reinforced with 20 wt% of B_4C. (Reproduced with permission from [150].) (b) XRD diffractograms of this composite under different processing variables. (Reproduced with permission from [150].) (c) HAADF-STEM image of the B_4C reinforcement surrounded by reaction products. (d) TEM image of the Al_3BC nanoparticles at the interface Al/B_4C (SAED pattern inserted). (e) HAADF-STEM image for the analysis of the Al_3BC/matrix interface. EDS mappings show the elements distribution. (f) High-resolution HAADF image of the Al_3BC particle, surrounded by a 0.7 nm Cu layer ((c)–(f) Reproduced with permission from [152].).

Si–0.25 Cu (wt%) alloy reinforced with 20 wt% of B_4C [150]. Interfacial reactions products for this composite were Al_3BC, Al_4SiC_4, $Mg_2B_2O_5$, Mg_2AlO_4, and MgB_7. This is shown in the XRD diffractogram of Figure 8b for the composite processed under different variables. Otherwise, reaction products surrounding B_4C can be observed in the high-angle annular dark field (HAADF)-STEM image of Figure 8c [152], for a 6061 Al alloy reinforced with 26 wt% of B_4C particles. These products formed a continuous layer consisting of polygonal nanoparticles (arrowed) at the interfacial region. Figure 8d shows that these nanoparticles correspond to Al_3BC, identified using SAED. Nanometric MgB_2 particles were also found (arrowed nanorod), formed in the matrix close to the B_4C reinforcement. HAADF-STEM and energy-dispersive X-ray spectroscopy (EDS) elemental mapping analyses of the Al_3BC nanoparticles showed a thin layer

of Cu surrounding the Al_3BC particle, as it is shown in Figure 8e. A high-resolution HAADF image of Figure 8f shows the bright contrast of this layer, which implies the presence of heavy Cu atoms. Cu and Mg were also segregated at the MgB_2/matrix interface. Segregation occurs to reduce the interfacial energy, enhancing nucleation rate and avoiding precipitate coarsening [152]. Al_3BC is reported as a hexagonal structure with lattice parameters a = 0.6046 nm and c = 1.154 nm [145]. This compound has been reported together with AlB_2, which also has a hexagonal structure, with a = 0.311 nm and c = 0.498 nm [145]. The crystal structure of B_4C is rhombohedra1 or hexagonal (a = 0.561 nm and c = 1.214 nm), differing from face-centered cubic structure of Al, a fact that diminish the possibility of getting a good bond directly between them, but the formation of these interfacial compounds favors bonding, significantly influencing the loading transfer between reinforcements and matrix, and consequently improving the mechanical properties of the composites [154]. This interlayer needs to be more studied to analyze their growth mechanism, orientation relationships, and other crystallographic characteristics.

As for the case of Al alloys reinforced with SiC, important research was found related to the interactions of these matrices with B_4C. These results show that again, Cu is the alloying element with the lowest interaction and reactions products when it is added to Al alloys. Its role and participation in different reactions are barely known, except its presence in precipitation processes. On the other hand, the use of Mg excels, increasing wettability and forming a wide variety of compounds, which increase the mechanical properties of the composite. Related to the addition of Si to these matrices, it is also beneficial because the formation of Al_4C_3 is avoided, obtaining SiC as a reaction product, which improves mechanical properties.

2.4 Boron nitride (BN)

BN exists in several polymorphic forms, outstanding cubic (c-BN) and hexagonal (h-BN) for reinforcing composites, although its use as coating is more common, presenting excellent wear and corrosion resistance. c-BN is considered the second hardest material next to diamond [17]. Its density is 3.45 g·cm^{-3}, and its bulk modulus is 400 GPa. Although h-BN and c-BN have been used together as reinforcements [155], h-BN (density of 2.25 g·cm^{-3}) excels [156]. According to the literature search, truly little interest has been paid to the use of BN particles reinforcing MMC due to the poor wettability for BN by almost all the molten metals [155,157,158].

2.4.1 BN in Al matrices

For Al matrices reinforced with BN, it has been reported the formation of AlN and AlB_2 in the interfacial region, by the following direct reaction [159]:

$$4BN_{(s)} + 5Al_{(l)} = 4AlN_{(s)} + 2B_{(l)} + AlB_{2(s)} \quad (31)$$

This reaction occurs for temperatures <985°C, while at higher temperatures it is reported [159]:

$$14BN_{(s)} + 15Al_{(l)} = 14AlN_{(s)} + 2B_{(l)} + \alpha AlB_{12(s)} \quad (32)$$

2.4.2 BN in Al matrices with Mg

Lee et al. [160] reported that the presence of Mg origins the formation of reaction products containing Al, Mg, and B, named Al(Mg)–boride. This is for an Al–4.5% Mg alloy reinforced by infiltration at 800°C with 5 and 7.5% h-BN particles. Besides, they reported the reaction between Mg and N to form Mg_3N_2 surrounding BN, which enhanced infiltration. Khatavkar et al. [161] reported that the wettability of h-BN was improved due to the addition of 1% Mg for a 2024 Al alloy. Reaction to form Mg_3N_2 can be summarized as follows [160,161]:

$$3Mg_{(l)} + 2N = Mg_3N_{2(s)} \quad (33)$$

After this reaction, Mg_3N_2 reacts with Al to obtain AlN according to:

$$Mg_3N_{2(s)} + 2Al_{(l)} = 2AlN_{(s)} + 3Mg_{(l)} \quad (34)$$

These reactions were also reported by Woo et al. [162], who besides found $MgAlB_2$.

2.4.3 BN in Al matrices with Mg and Si

Konopatsky et al. [163] found that for an Al–10 Si–Mg alloy with 1, 3, and 5 wt% of BN used for 3D printing (~2,627°C were reached during ~0.15 ms), there was the formation of AlN at the BN surface, while AlB_2 nanoparticles (~10 nm) were observed in the matrix near the interface. These authors did not report the effect of Si and Mg, or the formation of products due to reactions with these elements.

2.4.4 BN in Al matrices with Cu

The precipitation process can be also modified for Al alloys reinforced with BN, as it is observed in the TEM

images of Figure 9a and b for an Al–5Cu alloy, and for an Al–5Cu/5%BN composite, respectively, both aged at 200°C for 9 h [157]. As it is clearly noted, differences in the precipitates are significant: θ′-phase averaging ~200 nm in length and 20 nm in width precipitated for the Al–5 Cu alloy (Figure 9a), corresponding to age-peak, while the stable θ-phase with 500 nm in length and 200 nm in width precipitated for the Al–5Cu/5%BN composite (Figure 9b), corresponding to the overaging state. Besides, they found the formation of strong bonded Al/BN interfaces, without gaps; while AlB_2 was obtained as an interfacial product, without reactions involving the presence of Cu. An example of a well-bonded BN/Al matrix interface can be observed in Figure 9c and d for an Al–5.3Cu/3% hBN composite (in wt%) processed at 640°C through semi-solid powder metallurgy technique. Figure 9c shows a TEM image of the composite, while the HRTEM image of Figure 9d shows that BN was strongly bonded with the Al matrix, through a Al_2O_3 nanolayer formed due to the oxidation of Al. The presence of BN and the interfacial characteristics allowed to obtain elevated hardness, compressive strength, and fracture strain [156]. The aforementioned AlN and AlB_2 interfaces can be obtained even at temperatures slightly below the Al melting point, following two mechanisms: (i) transformations inside Al grains (AlB_2) or (ii) along the Al grain boundaries (AlN). Besides, Al_2O_3 often is obtained due to the substitution of N atoms by O in the growing AlN phase, being more favorable the formation of Al_2O_3 than AlN. h-BN has hexagonal crystal lattice, with a = 0.250 nm and c = 0.662 nm, with atoms of N of 0.146 nm, very similar to the ionic radius of O (0.140 nm), occurring this substitution. These factors also favor the formation of AlB_2, which has a hexagonal lattice with a = 0.301 nm and c = 0.325 nm, while AlN has a hexagonal structure, with a = 0.311 nm and c = 0.498 nm [160]. The preferential formation of the AlB_2 phase

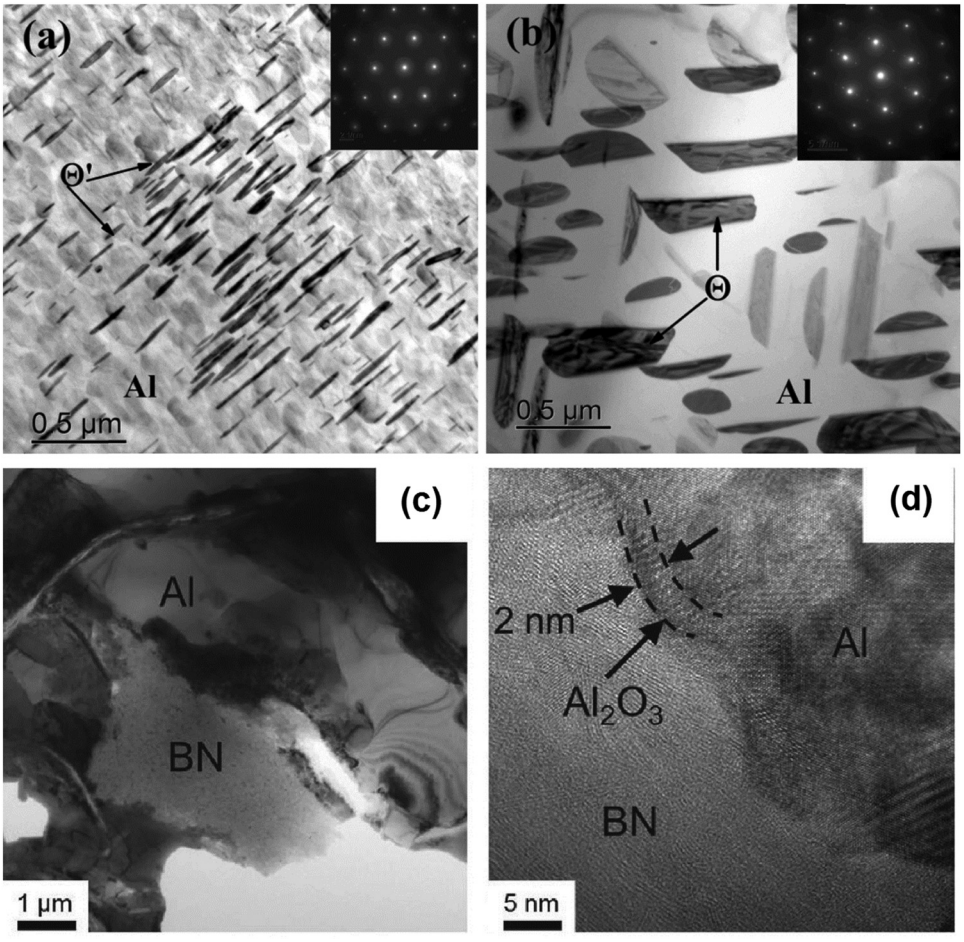

Figure 9: TEM images after aging 9 h at 200°C for: (a) an Al–5% Cu alloy and (b) an Al–5% Cu/5% BN composite. (Reproduced with permission from [157].) (c) TEM image for an Al–5.3 Cu/3 BN composite and (d) HRTEM image of this composite showing an $Al/Al_2O_3/BN$ interface (Reproduced with permission from [156].).

compared to AlN in the solid state could be explained because B atoms can more easily penetrate into the metallic Al lattice compared to N. Besides, the lattice mismatch for c parameter for BN/AlB_2 is 0.006 (by counting 1/2 for BN), which could lead to achieve some degree of semicoherency at their interface. At higher temperatures, the preferential formation of AlN occurs due to a more negative value of the Gibbs free energy [163].

Contrary to that observed for the aforementioned carbides, for BN, the information is limited, even for the interaction of this reinforcement with Al. Only research works with reactions involving Mg were reported, reporting that this element improves wettability and mechanical properties of the composite. The effects of Si and Cu were not found, although some works reported the use of Al matrices containing these elements. This shows that more research is needed for the use of BN as reinforcement and also shows its interactions with different Al matrices.

2.5 Silicon nitride (Si_3N_4)

Si_3N_4 has good thermal and chemical stabilities, high mechanical strength and hardness, and good wear resistance, not only improving the mechanical properties of Al alloys but also conferring to the composites better thermal and dimensional stabilities [164,165]. Its density is 3.44 g·cm^{-3}, with a hardness of 35 GPa [166].

2.5.1 Si_3N_4 in Al matrices

For the case of the interaction between molten Al and Si_3N_4, the following reaction has been reported at temperatures ranging from 827 to 1,027°C [97]:

$$Si_3N_{4(s)} + 4A1_{(l)} = 4A1N_{(s)} + 3Si_{(l)} \quad (35)$$

This reaction is followed by the dissolution of Si in liquid aluminum according to the equilibrium of equation (4). As happens for the equilibrium SiC-Si, in this case, Si_3N_4–Si can control the direction of this reaction, bonding directly an interface Si_3N_4/Al, or with the interfacial layer Si_3N_4/AlN/Al. Lu et al. [166] reported the formation of AlN even for an alloy with 10% Si at temperatures above 750°C, improving the mechanical properties of the composite until reaching 850°C. In this temperature range, a thin reaction layer led to increase in the interfacial bonding, improving hardness, fracture toughness, and flexural strength. The thickness of the reaction layer increased with the increase in the temperature due to a higher reactivity, but at temperatures above 850°C, the interface embrittlement deteriorated the mechanical properties. At this point, the fracture modes changed from ductile intergranular to brittle intergranular. At temperatures higher than 950°C, intense interfacial reaction occurred, and the composites became AlN and Si due to the complete consumption of Si_3N_4.

2.5.2 Si_3N_4 in Al matrices with Mg

Akhtar and Guo [167] studied a Si_3N_4/Al–2Mg composite manufactured by pressureless melt infiltration and reported the formation of AlN and $Al_{13.27}Si_{0.47}$. De la Peña and Pech-Canul [168] also reported these reaction products, and the formation of MgO and $MgAl_2O_4$, which reduced wetting through reactions involving Mg_3N_2, described as follows:

$$Si_3N_{4(s)} + 6Mg_{(l)} = 2Mg_3N_{2(s)} + 3Si_{(l)} \quad (36)$$

This reaction is followed by other reactions that lead to the lack of wetting:

$$2Mg_3N_{2(s)} + 3O_{2(g)} = 6MgO_{(s)} + 2N_{2(g)} \quad (37)$$

$$Mg_3N_{2(s)} + 6O_{2(g)} + 6Al_{(l)} = 3MgAl_2O_{4(s)} + N_{2(g)} \quad (38)$$

Besides, it is reported that the surface of Si_3N_4 can be covered by Si_2N_2O due to the interaction of the reinforcement with O_2. Then, the reaction Al alloy/Si_3N_4 is substituted by a reaction including Si_2N_2O instead of the original reinforcement, being as follows [168]:

$$4Si_2N_2O_{(s)} + 2Al_{(l)} + Mg_{(l)} = MgAl_2O_{4(s)} + 2Si_3N4_{(s)} + 2Si_{(in\ l\ Al)} \quad (39)$$

Koike et al. [169] reported partial melting at matrix/Si_3N_4 interfaces and at the grain boundaries of the matrix for temperatures as low as 450°C. This occurred for an Al–2.46 Mg alloy reinforced with 20% Si_3N_4 particles. The cause of this behavior was the segregation of Mg and Si to interfaces and grain boundaries, decreasing solidus temperature. The effect of Mg additions was also studied by Wang et al. [170], who analyzed the infiltration kinetics of Si_3N_4/Al–Mg composites fabricated by pressureless infiltration. These authors found that the increase in the Mg content from 2 to 10 wt% significantly improved the infiltration process. Nevertheless, for higher Mg contents, they reported an adverse effect due to interfacial reactions, forming Mg_2Si, MgO, and Al_2O_3. As can be seen, a nonheat treatable Al–Mg alloy was modified to a heat-treatable Al–Si–Mg alloy due to the Si released (equations (35), (36) and (39)), being possible for the precipitation of Mg_2Si according to the following equation:

$$2\,Mg_{(l)} + Si_{(l)} = Mg_2Si_{(s)} \quad (40)$$

In addition, the presence of oxides increases melt viscosity and deteriorates the wettability of the system matrix/reinforcement [171]. The reactions to obtain these different oxides include equations (37)–(39), in addition to [170,172]:

$$Si_3N_{4(s)} + O_{2(g)} = 3SiO_{2(s)} + 2N_{2(g)} \quad (41)$$

2.5.3 Si_3N_4 in Al matrices with Cu and Mg

Figure 10a shows a SEM image with the microstructure of a squeeze cast Al–5Cu/7% Si_3N_4 alloy composite, where Si_3N_4 particles (dark gray) and Al_2Cu phase (light) are clearly differentiated [157]. Besides, AlN (intermediate grey scale) is observed surrounding Si_3N_4, formed according to the reaction of equation (35). Its presence was corroborated through the XRD analysis shown in Figure 10b, where peaks belonging to Al, Si_3N_4, Al_2Cu, and AlN can be identified. This or other interfaces can be formed depending on the presence of Mg. Jeong et al. [173] studied the mechanical properties and interfacial characteristics of Al–Cu and Al–Cu–Mg alloys reinforced with Si_3N_4. They found that the composites with Al–Cu–Mg matrices presented significantly higher elongations than Al–Cu composites, and this is due to the absence of cavities at the interfacial regions and a stronger interface for Al–Cu–Mg matrices. These authors used TEM to analyze the interfaces Al/Si_3N_4 after tensile deformation and found significant differences between them. As shown in Figure 10c, Al/Si_3N_4 interface for the composite with Al–Cu matrix presented flat edges without interfacial reaction products. Its analysis using HRTEM showed a thin SiO_2 amorphous layer of about 1 nm covering the interface (arrowed). The formation of this layer suggests no reaction Al/Si_3N_4. Otherwise, Figure 10d shows that interfaces for the composite with Al–Cu–Mg matrix presented curved surfaces and interfacial reaction products, indicating a strong reaction. In this case, the SiO_2 amorphous layer was not reported. Reactions products (arrowed) grew with definite crystallographic relationships to Si_3N_4 and were discontinuously located surrounding Si_3N_4. EDS and crystallographic analyses showed that the reaction phase was a fcc. Al-based solid solution was supersaturated by Si and Mg. These reaction phases grew with definite crystallographic relationships to the Si_3N_4 crystal, which has a cubic lattice (a = 0.779 nm), whit a lattice mismatch Al/Si_3N_4 of 0.015 (by counting 1/2 for Si_3N_4), because for Al, a = 0.405 nm. This interface relaxed the stress concentration and suppressed the extensive development of microcracks and cavities. These results show the importance

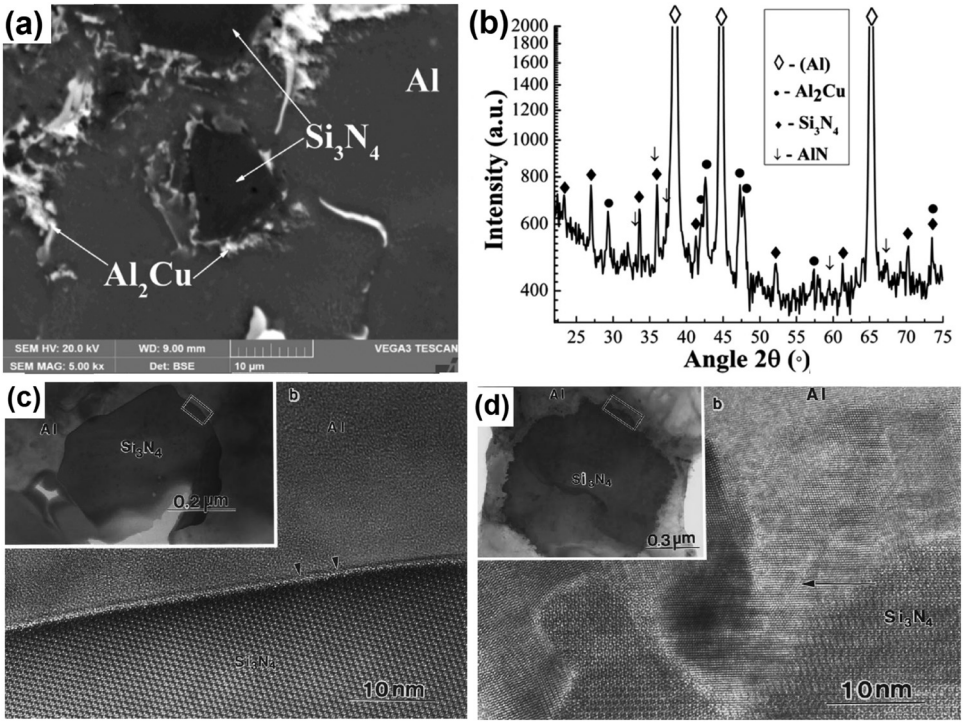

Figure 10: (a) SEM image of a squeeze cast Al–5 Cu/7% Si_3N_4 composite and (b) XRD analysis of this composite with the presence of different peaks. (Reproduced with permission from [157].) (c and d) TEM and HRTEM images of Si_3N_4 particles for tensile deformed. (c) Al–Cu/Si_3N_4 composite and (d) Al–Cu–Mg/Si_3N_4 composite (Reproduced with permission from [173].).

of Mg in these composites. HRTEM images were essential to analyze these crystallographic characteristics of the interfaces and revealed their effect on the mechanical properties of the composites.

2.5.4 Si_3N_4 in Al–Si–Cu–Mg matrices

Feng et al. [174] studied an Al–11.5Si–1.3Mg–1.3Cu–1.3Ni (max. wt%) alloy reinforced with 20% of Si_3N_4 whiskers, manufactured by squeeze casting, and found that the addition of the reinforcement modified α-Al morphology from dendritic to equiaxed. They also reported the modification of the eutectic Al–Si from netlike to particulate. In addition, MgO and $MgAl_2O_4$ were obtained as reaction products. These authors found that the increase in the manufacturing temperature led to stronger interfaces due to the segregation of solute atoms near this zone.

Chen et al. [175] reported that the addition of 45% Si_3N_4 accelerated the precipitation process of Al_2MgCu for an Al 2024 alloy (4.79 Cu–1.49 Mg–0.168 Si), although the precipitation sequence was not altered. Qu et al. [171] also reported a more accelerated kinetics for Mg_2Si precipitation, for an Al–11.5 Si–1.0 Mg–0.5 Cu–0.5 Ni alloy reinforced with 20 vol% of Si_3N_4 whiskers.

As for the other nonoxide reinforcements analyzed earlier, the study of Mg outstands as the alloying element for Al matrices reinforced with Si_3N_4, increasing wettability and forming compounds such as MgO and spinel $MgAl_2O_4$. Although some works analyze Si-rich matrices, the effect of this element on the equilibrium needs more attention. Otherwise, the presence of Cu as the reaction product was not found.

2.6 Carbon material reinforcements

In this section, we are presenting carbon materials reinforcing aluminum (C/Al). Among these reinforcements, we are including graphite, graphene, and CNTs, all of them presenting poor wettability by Al. Besides, they participate in similar reactions with Al and its alloys. The improvement of the mechanical properties attributed to carbon reinforcements is higher compared to the improvement reached for other ceramics, also decreasing friction coefficient and maintaining good electrical conductivity [51]. It has been reported that the combination between metals and graphitic carbon will outstand as the composite system [176]. Although some research can be found in the literature on the use of Al–Si–Cu–Mg alloys reinforced with C materials, few of these works study the effect of the alloying elements. Almost all works are focused on the effect of the reinforcement addition on the mechanical properties, e.g., the works of Reddy and Anand [177] and Abbasipour et al. [178]. In the following sections, some of these carbon materials and their interactions with these matrices were included.

2.6.1 CNTs

CNTs have low density and high strength-to-weight ratio and elevates ductility and corrosion resistance. They are used for reinforcing AMC in applications such as gears, cylinder liners, and sport utilities [17]. Polymer composites reinforced with CNT have been widely studied [179,180], but research related to the use of CNT reinforcing aluminum and its alloys is limited [19,43–45]. Among the topics needing attention for these composites are the interfacial bonding CNT/Al and the effect of the alloying elements on other interactions. It has been reported that atoms in graphitic structures in general present strong covalent s-bonds within a basal plane, also forming covalent bonds with metals [176]. In the case of CNTs, there are two different interfaces depending on the contact area of the CNT with the metal: (i) the contact with the ends of the CNT, involving covalent bonds at the interface, and (ii) a side-contact generating a weak bond [176].

2.6.1.1 CNT in Al matrices

For the system CNT/Al, it has been reported the formation of different carbides, significantly affecting the mechanical behavior of the resulting composites [19,43–45]. Wu and Kim [181] found the formation of carbides at temperatures higher than 620°C, affecting the interfacial bonding between CNTs and matrix. When molten aluminum reacts with carbon, the formation of Al_4C_3 can occur, as for other carbide/Al reactions presented earlier (see equations (1), (14), (17)), in this case through the following equation:

$$4/3\ Al_{(l)} + C_{(s)} = 1/3Al_4C_{3(s)} \quad (42)$$

Ci et al. [182] recommended that the processing temperature for manufacturing Al/CNT composites should be controlled below the melting point of the aluminum alloy. If this condition is not considered, a severe reaction Al/CNT may occur, significantly decreasing the mechanical properties of CNTs and the whole composite. At lower

temperatures, the formation of a thin Al_4C_3 layer occurs along the CNTs and at their ends, increasing mechanical properties due to a better stress transfer from the Al matrix [182]. Zhou et al. [183] found that the formation of Al_4C_3 is directly proportional to the processing temperature, reaching 100% at the melting point of aluminum. Once Al_4C_3 appears, it acts as a barrier for further reaction to occur. Initially, a thin and uniform carbide coating appears, followed by an uninterrupted consumption of the CNT until its complete reduction to obtain a solid Al_4C_3 nanowire [42]. Its growth can be both perpendicular and lateral by the diffusion of Al toward the CNT and C toward the Al matrix.

2.6.1.2 CNT in Al matrices with Si

Several studies have shown that matrix composition has a significant effect on the reaction products and on the kind of interfacial layer formed. Bakshi et al. [46] reported the formation of two different carbides due to the reaction between CNT and molten metal: Al_4C_3 for an Al–11.6 wt% Si alloy, and SiC for an Al–23 wt% Si alloy. For Al–Si alloys, SiC is formed through the reaction:

$$Si_{(l)} + C_{(s)} = SiC_{(s)} \tag{43}$$

The mechanism of growth of SiC is similar to the formation of Al_4C_3 and begins with C atoms reacting with Si, forming a very thin SiC layer [43]. Its growth also includes lateral growth on the CNT surface and perpendicular growth to the formed carbide layer. The formation of Al_4C_3 or SiC depends on both temperature and Si content, as it is reported in different works [43,46,184]. Bakshi et al. [46] reported that for a 11.6 wt% Si Al alloy, the critical carbide thickness for the formation of Al_4C_3 is lower than for the formation of SiC, while it is inverse for a 23 wt% Si alloy. They presented a graph with the equilibrium fraction of $Al_4C_3/(Al_4C_3 + SiC)$ vs Si wt% in the alloy, at various temperatures, for composites reinforced with 10 wt% of CNTs. This diagram can be used to predict the interfacial carbide formed according to alloy matrix at a given processing temperature. Although the formation of small amounts of Al_4C_3 is helpful in stress transfer to CNTs by pinning the CNT to the matrix [185,186], it is preferred the formation of SiC. Critical layer thickness for SiC formation is lower than that for Al_4C_3 formation, which leads to a better wettability of molten Al-Si matrix with CNT. Al/SiC has a higher work of adhesion, indicating a lower contact angle for wetting. Besides, interfacial strength is higher when SiC is formed, presenting a more efficient load transfer for Al_4C_3, preventing delamination [43]. Figure 11a and b shows high-resolution TEM images for the analysis of the formation of these carbides [46]. As shown in Figure 11a, a thin (2–5 nm) layer of SiC is present on the CNT surface, for an Al–23 wt% Si alloy reinforced with 10 wt% CNTs. Otherwise, the formation of Al_4C_3 occurred for a matrix with lower Si content, as shown in Figure 11b for an Al–11.6 wt% Si alloy. Crystallographic planes corresponding to Al, Si, and Al_4C_3 can be identified in Figure 11b. It has been reported a defined orientation relationship between Al_4C_3 and C in other C materials, but this does not occur for CNTs due to the structural configuration of the carbide. This Al_4C_3 layer has a rhombohedral structure, with alternate Al_2C and Al_2C_2 layers, with a = 0.3335 nm, b = 0.3335 nm, and c = 0.85422 nm. Thus, Al_4C_3/CNT interface is expected to be strained due to the higher C–C distance in Al_4C_3 (3.33 Å) compared to this distance in CNT (1.42 Å) [46].

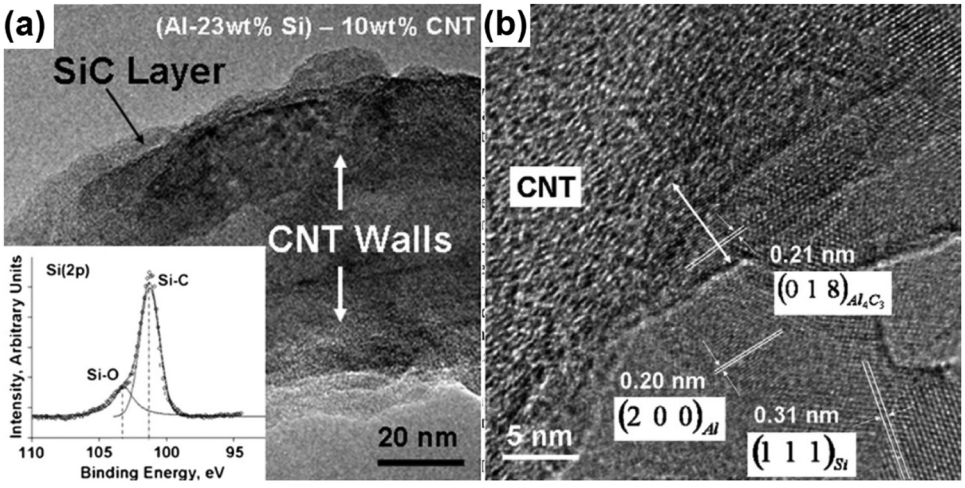

Figure 11: High-resolution TEM images of (a) an Al–23 wt% Si alloy reinforced with 10 wt% CNTs (inset shows the XPS validating SiC) and (b) an Al–11.6 wt% Si alloy containing 10 wt% CNT (Reproduced with permission from [46].).

2.6.1.3 CNT in Al–Si–Cu–Mg matrices

For these alloys, different interactions can occur. Abbasipour et al. [187] reported that the addition of 1%Mg (in mass) originated a higher wettability for an A356 Al–7Si–0.3Mg alloy reinforced with CNTs, stirred at 700°C. Elshalakany et al. [188] found grain refinement with the increase in the CNTs content for an A356 (6.6 Si, 0.30 Mg, 0.27 Fe, and 0.020 Cu) alloy reinforced with 2.5 wt% of CNT. On the other hand, Deng et al. [189] reported that at temperatures above the melting point of an Al–4.20 Cu–1.47 Mg (in wt%) alloy, CNTs reacted with aluminum and formed Al_4C_3. These authors did not report any reaction between Cu or Mg with CNTs.

The formation of other carbides has been reported for these composites, but only after being heat treated. Kondoh et al. [190] reported Al_2MgC_2 for a T6 heat-treated Al–0.58 Si–0.57 Mg–0.08 Fe (in wt%) alloy, reinforced with 1% CNT. Al_2MgC_2 precipitated due to Mg diffusion toward the CNTs, resulting in a lower matrix hardening by the incomplete precipitation of Mg_2Si. These authors also found that the reduction of the Mg content, needed to precipitate Mg_2Si, may be originated by the adsorption of elemental O by the CNTs, forming MgO and $MgAl_2O_4$ (spinel). The reaction to form Al_2MgC_2 could be resumed as follows:

$$2\,Al_{(l)} + 2C_{(s)} + Mg_{(l)} = Al_2MgC_{2(s)} \quad (44)$$

Modifications of the precipitation processes were found in the literature for the reinforcement of these alloys with CNT. Nam et al. [191] reported that aging kinetic was enhanced with the increase in the CNT content for an Al–Cu matrix, while Choi et al. [192] reported that the aging peak appeared for a time significantly lower for a AA2024/CNT composite than for the unreinforced matrix. Meng et al. [193] also found that comparing with an unreinforced Al-Cu alloy, peak aging time decreased after reinforcing this alloy with CNTs. Fukuda et al. [194] found a similar behavior for an Al–Mg–Si alloy, reporting that the addition of 1.22 vol% CNTs to the alloy significantly decreased precipitation of Mg_2Si. The reduction of the precipitation process for this matrix reduced the strength of the composite, attributed to the depletion of Mg from the matrix due to its segregation to CNT clusters [194,195].

As mentioned earlier, the effect of Si additions is well known, contributing to form SiC instead of Al_4C_3, while Mg can contribute to obtaining different reaction products and increases wettability. Nevertheless, more research is necessary for the contribution of this element to the interfacial reactions. Finally, the effect of Cu was not found, although some works reported the use of Al matrices containing it. These results demonstrate that more research is needed for the use of CNT as reinforcement, in composites with Al matrices containing these alloying elements.

2.6.2 Other carbon material reinforcements

CNTs are the most used C material for reinforcing Al, but there are few works about the use of graphene and graphite. That is why we are including a brief analysis of our search for these reinforcements.

Graphene has high mechanical, electrical, and thermal properties, reinforcing AMC and leading to better functional and mechanical properties. Graphene/Al composites have applications in catalysis, electronics, energy storage and conversion, sensing, and biotechnology [48]. Although this composite is more feasibly manufactured by powder metallurgy, avoiding interfacial reactions [20], Chak and Chattopadhyay [49,50] reported the use of stirring-assisted liquid route for manufacturing AMC of graphene nanoplatelets reinforcing an Al matrix. Graphene addition acted as grain refiner and improved mechanical and wear properties, although agglomeration occurred for graphene wt% >0.5. The bonds between Al, Cu, and other metals with graphene are weak Van der Waals forces, leading to the agglomeration of the reinforcements. These agglomerated layers form thick sheets and generate interfacial defects. Besides, Al_4C_3 may be obtained [196], decreasing the composite properties. This reinforcement has been less studied than other C materials and needs more attention. No works were found related to the formation of other carbides or reaction products due to the addition of Si, Cu, or Mg to Al matrices reinforced with graphene.

On the other hand, graphite has low density, high thermal conductivity, and good mechanical strength, reinforcing Al alloys in applications such as heat sinks, brake discs, and pistons [17]. The interaction of Al with graphite also origins the formation of Al_4C_3. This reaction is severe at temperatures higher than 627°C, degrading the reinforcement and leading to a decrease in strength [17,196]. Liu et al. [196] found that the addition of small amounts of Mg prevents the formation of graphite clusters, leading to composites with improved physical and mechanical properties. They obtained a composite with graphite particles uniformly distributed in an Al–0.6 wt% Mg matrix, but when Mg content increased to 1 wt%, agglomeration took place. Pelleg et al. [197] investigated the effect of alloying elements on the Al/graphite interface and found that Si presented the highest effectivity as the alloying element for avoiding or reducing the formation of Al_4C_3. They reported that Mg is also efficient in reducing the solubility of C in Al. Although for graphite

exists more information than for graphene, this reinforcement also needs attention.

2.7 Fe

Although some works use Fe particles to reinforce Al, this reinforcement is preferentially used as hollow spheres reinforcing Al syntactic foams [56–59]. The analysis of the interactions Al Fe/matrix is detailed next.

2.7.1 Fe in Al matrices

Some reported reactions when molten Al comes in contact with solid Fe are as follows [58,198,199]:

$$Fe_{(s)} + Al_{(l)} = FeAl_{(\text{liquid solution})} \quad (45)$$

$$Fe_{(s)} + 3Al_{(l)} = Al_3Fe_{(s)} \quad (46)$$

The Fe–Al system can form six nonstoichiometric intermetallic compounds: $AlFe_3$, AlFe, Al_2Fe, Al_3Fe_2, Al_5Fe_2, and Al_3Fe [200]. Some of them have been reported for these syntactic foams for different matrices. Lee et al. [199] studied the reinforcement of Al by 10% of Fe particles through the friction stir process, identifying that reaction products were $Al_{13}Fe_4$ (also denoted as Al_3Fe) and a low quantity of Al_5Fe_2. This last compound was obtained due to the reaction between $Al_{13}Fe_4$ and Fe. Other Fe–Al and ternary intermetallics have been reported, but mainly for Si-rich matrices, as will be analyzed next.

2.7.2 Fe in Al matrices with Si

The use of Fe reinforcing AMCs has been mainly researched for Al–Si alloys. The same occurs for MMSF, where almost all the studies are related to the infiltration method. Si imparts excellent castability to Al alloys, also leading to the formation of different intermetallics Al–Fe–Si. Ten different ternary intermetallics have been reported for this system [201]. Guo et al. [202] reported an intermetallic layer for an Al–7 Si alloy reinforced with Fe hollow spheres, with three different compositions in the interfacial region: Al_5Fe_2, Al_3Fe, and Al_8Fe_2Si. The increase in the interface thickness led to the fast fracture of the Al/Fe bonding. A brittle-hard needle-like phase (Al_5FeSi) in the Al matrix around Al/Fe interface was the main cause of the lower shear strength. Rabiei and Vendra [59] studied MMSF consisting of low-carbon steel hollow spheres, reinforcing an Al-7Si alloy. They used casting processing, reporting the formation of an $Fe_{25}Al_{60}Si_{15}$ interfacial layer and of hard Fe_2Al_7Si plates. The formation of the interfacial layer increased the bonding strength between spheres and matrix, improving the mechanical properties of the material. For Al–7Si matrices, Vendra and Rabiei [203] and García-Avila and Rabiei [204] found different intermetallics and the same interfacial layer. This can be observed in the SEM images of Figure 12a and b. As shown in Figure 12a, needle-shaped $FeAl_4Si$ is present in the Al–Si matrix, while Figure 12b shows a continuous interfacial layer of $Fe_{25}Al_{60}Si_{15}$ surrounding the sphere and an intermediate discontinuous layer of block-like Fe_2Al_7Si particles. Due to the presence of such intermetallic phases, these syntactic foams present brittle fracture. Al and Si interdiffusion from the matrix to the sphere walls have been reported, also diffusing Fe and other alloying elements from the sphere toward the matrix. This leads to the formation of different ternary intermetallics with hexagonal or more complex crystal structures. The crystallographic analysis in the literature of $Fe_{25}Al_{60}Si_{15}$ (τ10-phase $Fe_5Al_{12}Si_3$) showed a hexagonal lattice for this intermetallic, with $a = 0.753$ nm and $c = 0.763$ nm [205]. Fe has bcc crystal lattice, with $a = 0.2866$ nm, while as commented earlier for

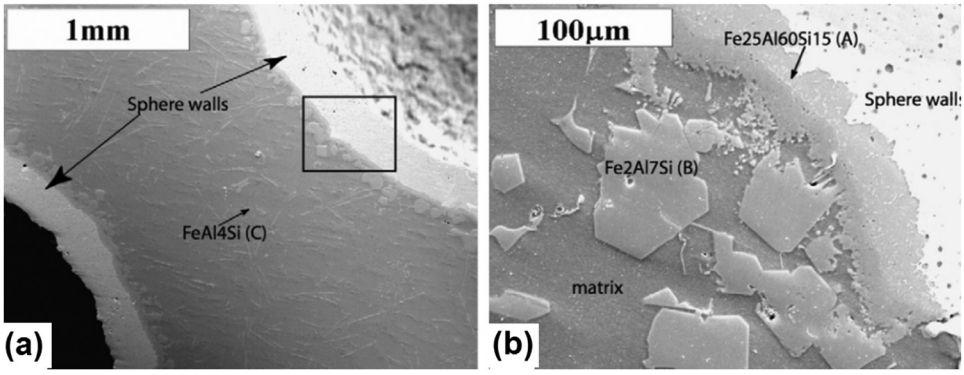

Figure 12: SEM images of an Al–12Si alloy reinforced with hollow steel spheres, processed by casting. (a) Spheres with their walls, and matrix with FeAl4Si are clearly observed. (b) Sphere/matrix interface with the presence of different phases (Reproduced with permission from [59].).

Al a = 0.405 nm. This could lead to poor coherency among Al, Fe, and the intermetallic layer, with few orientation relationships. These characteristics need more attention for these materials, including their study through techniques such as HRTEM, because this and other interfaces are only shown using SEM or OM, and identified using XRD, without a more in-depth analysis [58,202,203].

2.7.3 Fe in Al–Si–Cu–Mg matrices

Bálint and Szlancsik [206] studied syntactic foams formed by matrices Al99.5, Al–12 Si, Al–1 Mg–1 Si, and Al–5 Cu, reinforced with Fe hollow spheres. They found that spheres had no significant impact on the microstructure of the matrix material, but coherent thin interfacial layers were observed for all the matrices. These layers presented strong bonding, which were beneficial for the mechanical properties. Near the spheres, the number of Si-, Cu-, and Mg-rich precipitates increased (for Al–12 Si, Al–5 Cu, and Al–1 Mg–1 Si matrices, respectively), while for composites with Al–5 Cu and Al–1 Mg–1 Si matrices, the sphere walls were enriched with Cu and Mg. Cu was found to be the element that most strengthened the foams, forming Al_2Cu.

Otherwise Orbulov and Ginsztler [207] found a significant effect of the alloying elements on the mechanical properties of MMSF with different matrices, being the best mechanical properties in the ascendant order Al99.5, Al–1 Si–1.2 Mg, Al–12 Si and Al–4.5 Cu. These authors also found that T6 heat treatments led to strength increments much smaller than expected due to the lower precipitation. The cause of this modification in the aging process was the decrease in the alloying elements in the matrix, originated by the interfacial reactions and the diffusion of alloying elements to the spheres.

Due to the hollow interior of the spheres, their interfaces with the matrices represent a high fraction of the solid material of a syntactic foam, as reported by Vendra and Rabiei [208]. They found that for an Al 356 alloy, reinforced with 59 vol% of steel hollow spheres, the volume of the Al–Fe–Si intermetallic layer represented 7% of the whole composite. That is why in this kind of composites, the effect of the interface is more determinant on the mechanical properties.

As can be seen, enough information was found in the literature for the reactions between Fe spheres and Al or Al–Si matrices, with different reaction products. Nevertheless, it was noted that more research is needed about the effect of the manufacturing process on the interfacial reactions. For alloys with the presence of Cu and/or Mg, the information is few and mainly focused on the modification of the precipitation processes due to the addition of the reinforcements. That is why, for the use of Fe as reinforcement, it is also essential to increase research in relation to the addition of these alloying elements and direct or indirect effects on microstructure and mechanical properties. Although Fe–Al intermetallics and interfaces are well known, including their crystallographic analyses, more attention is necessary for their formation and characteristics for the specific case of syntactic foams and their manufacturing processes.

3 Summary and outlook

Table 1 presents a recompilation of the reaction products obtained due to the interactions between nonoxide reinforcements and Al matrices with the presence of Si, Cu, and/or Mg as alloying elements. The variety of compounds can be obtained. Nevertheless, their studies

Table 1: Reaction products for different reinforcements in Al and Al–Si–Cu–Mg matrices

Reinforcement	Reaction products for pure Al matrices	Other reaction products for Al–Si, Cu and/or Mg matrices
SiC	Al_4C_3, SiO_2, Al_2O_3	Mg_2Si, MgO, $MgAl_2O_4$
WC	Al_5W, $Al_{12}W$, Al_4C_3, Al_4W, W_2C	No products found
B_4C	B_2O_3, $AlB_{40}C_4$, $Al_2B_{48}C_8$, $Al_2B_{51}C_8$, $Al_3B_{48}C_8$, $Al_8B_4C_7$, $B_{12}(B,C,Al)_3$, Al_3BC, AlB_2, AlB_{10}, $Al_2B_4C_4$, $Al_3B_{48}C_2$, $Al_{12}BC_2$, Al_4C_3	$Al_xMg_{(1-x)}B_2$, MgB_6, $(Al,Mg)B_2$, $MgAl_2O_4$, MgB_2, SiC, MgO, MgB_7, Al_4SiC_4, $Mg_2B_2O_5$
BN	AlN, AlB_2, AlB_{12}	Mg_3N_2, $MgAlB_2$,
Si_3N_4	AlN, SiO_2	Mg_3N_2, MgO, $MgAl_2O_4$, $Al_{13.27}Si_{0.47}$, Si_2N_2O, Mg_2Si, Al_2O_3
C-reinforcements	Al_4C_3	SiC, Al_2MgC_2, MgO, $MgAl_2O_4$
Fe	FeAl, Al_3Fe, $AlFe_3$, Al_2Fe, Al_3Fe_2, Al_5Fe_2	Al_8Fe_2Si, Al_5FeSi, $Fe_{25}Al_{60}Si_{15}$, Fe_2Al_7Si, $FeAl_4Si$

focused on some reinforcement/alloy systems, as it is remarked next.

From this table and after the analysis of other interactions presented in this work, some remarks about the interactions between nonoxide reinforcements and Al–Si–Cu–Mg matrices are as follows:

Among the modifications originated in the Al matrices due to the additions of these reinforcements, we found the refinement of the grain size and the microstructure in general, also modifying matrix precipitation process due to diffusion and interfacial reactions, which can lead to different contents of alloying elements in the matrix. An individual study of each combination reinforcement/matrix is needed, mainly including the alloying elements content and their possible combinations.

Related to the interfacial reactions, the conditions for their occurrence are different and highly dependent on the temperature and composition of the matrix. For some reinforcements such as SiC and B_4C, the reactions and interactions are well studied; but for others such as BN, graphite, and graphene, the information is limited or inexistent. Among the alloying elements, the study of Mg excelled, with an important quantity of reaction products for almost all the reinforcements, highlighting the formation of MgO and spinel $MgAl_2O_4$. It was found that the addition of Mg generally leads to an improvement of wetting, increasing the interfacial bonding and hence the mechanical properties. Nevertheless, for each case, the analysis of the effect of not only this alloying element on wetting but also on the agglomeration of the reinforcements is necessary. The crystallographic analysis of the interfaces reinforcement/matrix using techniques such as XRD, HRTEM, and SAED allows to link their characteristics with the mechanical properties of the composite.

For carbides, relevant information was found for the use of SiC and B_4C as reinforcements, with different reactions. Nevertheless, WC presents low reactivity with these matrices, with few reaction products due to the interaction WC/Al, and no products found in the literature involving Si, Cu, or Mg. The addition of Si to the Al matrices leads to minimize or even avoiding the formation of harmful Al_4C_3 for carbide reinforcements, forming different reaction products (except for WC).

For nitrides, works found in the literature did not report the effect of Si and Cu, or the formation of products due to reactions with these elements, while the addition of Mg leads to obtain some reaction products, but not as extended as the observed for SiC and B_4C. For Si_3N_4, reactions have been more studied than for BN, with the formation of different Mg-rich compounds, including MgO and the spinel phase.

The information is scarce for the interactions between carbon reinforcements and these matrices, with some works just for CNTs. For these composites, the effect of Si additions is like the reported for carbides, leading to minimize or even avoid the formation of harmful Al_4C_3, also forming different reaction products. Few reaction products including Mg were found for these reinforcements, also including MgO and spinel, while the effect of Cu was not found.

Finally, for composites reinforced with Fe, the information is wide, mainly for alloys including Si due to the use of this element improving casting. Different Al–Si–Fe compounds are reported as reaction products, significantly affecting mechanical properties. Contrary to the observed for other reinforcements, in the case of Fe, no information was found related to the effect of Mg and Cu. No interfacial reactions were reported involving these elements. No studies were found about the crystallographic analysis of the interfaces Fe/Al matrices.

3.1 Future research directions

Derived from these conclusions, it is important to note some punctual directions to follow related to the research of these combinations of reinforcements and matrices. A first research topic could be the interactions of pure Al matrix with WC, BN, and carbon material reinforcements, for different manufacturing temperatures. A second topic could be the effect of adding different amounts of Si and Cu to these matrices (Mg has been more studied for these reinforcements). A third research topic is related to the effect of Mg and Cu on the interactions between Al–Si matrices and Fe. In all these studies, the crystallographic study of the interfaces is essential.

Acknowledgments: The support of Departamento de Ingeniería de Procesos e Hidráulica, Universidad Autónoma Metropolitana-Iztapalapa is acknowledged.

Funding information: I. Alfonso acknowledges the financial support from PASPA DGAPA-UNAM. This work was also supported by SEP-CONACYT 285215 and UNAM-PAPIIT IN102322 projects.

Authors contributions: Ismeli Alfonso: writing – original draft, project administration, funding acquisition, writing – review and editing, methodology, formal analysis; Federico González: writing – original draft, formal analysis, visualization; Tania E. Soto: investigation, methodology; Joel

Vargas: supervision, validation resources, visualization, project administration; Claudio Aguilar: methodology, validation, formal analysis; Ignacio A. Figueroa: writing – review and editing, methodology, formal analysis; Gonzalo González: methodology, validation, and formal analysis. All authors have accepted responsibility for the entire content of this manuscript and approved its submission.

Conflict of interest: The authors state no conflict of interest.

References

[1] Pasha, M. B. A. and M. Kaleemulla. Processing and characterization of aluminum metal matrix composites: an overview. *Reviews on Advanced Materials Science*. Vol. 56, No. 1, 2018, pp. 79–90.

[2] Baumli, P. Interfacial aspects of metal matrix composites prepared from liquid metals and aqueous solutions: A Review. *Metals*. Vol. 10, No. 10, 2020, id. 1400.

[3] Hashim, H., M. S. Salleh, and M. Z. Omar. Homogenous dispersion and interfacial bonding of carbon nanotube reinforced with aluminum matrix composite: A review. *Reviews on Advanced Materials Science*. Vol. 58, No. 1, 2019, pp. 295–303.

[4] Casas, B. Y., J. C. Carranza, I. A. Figueroa, J. G. González, O. Hernández, L. Béjar, et al. Fractal and conventional analysis of Cu content effect on the microstructure of Al–Si–Cu–Mg Alloys. *Materials Research*. Vol. 23, No. 4, 2020, id. e20190666.

[5] Alfonso, I., G. González, G. Lara, M. Rodríguez, M. Domínguez, M. G. Téllez, et al. Fractal analysis of the heat treatment response for multiphase Al alloys. *Materials Research*. Vol. 19, No. 3, 2016, pp. 628–639.

[6] Ibrahim, M .F., E. Samuel, A. M. Samuel, A. M. A. Al-Ahmari, and F. H. Samuel. Metallurgical parameters controlling the microstructure and hardness of Al–Si–Cu–Mg base alloys. *Materials and Design*. Vol. 32, No. 4, 2011, pp. 2130–2142.

[7] Zheng, Y., W. Xiao, S. Ge, W. Zhao, S. Hanada, and C. Ma. Effects of Cu content and Cu/Mg ratio on the microstructure and mechanical properties of Al–Si–Cu–Mg alloys. *Journal of Alloys and Compounds*. Vol. 649, 2015, pp. 291–296.

[8] Alfonso, I., C. Maldonado, G. Gonzalez, and A. Bedolla. Effect of Mg content and solution treatment on the microstructure of Al–Si–Cu–Mg alloys. *Journal of Materials Science*. Vol. 417, 2006, pp. 1945–1952.

[9] Farkoosh, A. R. and M. Pekguleryuz. Enhanced mechanical properties of an Al–Si–Cu–Mg alloy at 300°C: Effects of Mg and the Q-precipitate phase. *Materials Science and Engineering: A*. Vol. 21, 2015, pp. 277–286.

[10] Farahany, S., N. A. Nordin, A. Ourdjini, T. Abu Bakar, E. Hamzah, M. H. Idris, et al. The sequence of intermetallic formation and solidification pathway of an Al–13Mg–7Si–2Cu *in-situ* composite. *Materials Characterization*. Vol. 98, 2014, pp. 119–129.

[11] Samuel, F. H. Incipient melting of Al5Mg8Si6Cu2 and Al2Cu intermetallics in unmodified and strontium-modified Al–Si–Cu–Mg (319) alloys during solution heat treatment. *Journal of Materials Science*. Vol. 33, 1998, pp. 2283–2297.

[12] Soto, T. E., F. González, C. Aguilar, L. Béjar, I. A. Figueroa, M. Abatal, et al. Particularities of the formation and modification of Si and Mg_2Si as second phases in casting Al alloys: Use of shape descriptors and fractal dimension. *Transactions of the Indian Institute of Metals*, 2022, doi: 10.1007/s12666-022-02631-4.

[13] Nordin, N. A., S. Farahany, A. Ourdjini, T. A. A. Bakar, and E. Hamzah. Refinement of Mg_2Si reinforcement in a commercial Al–20%Mg_2Si *in-situ* composite with bismuth, antimony and strontium. *Materials Characterization*. Vol. 86, 2013, pp. 97–107.

[14] Azarbarmas, M., M. Emamy, J. Rassizadehghani, M. Alipour, and M. Karamouz. The influence of beryllium addition on the microstructure and mechanical properties of Al–15%Mg_2Si *in-situ* metal matrix composite. *Materials Science and Engineering: A*. Vol. 52828, 2011, pp. 8205–8211.

[15] Aravind, M., P. Yu, M. Y. Yau, and D. H. L. Ng. Formation of Al_2Cu and AlCu intermetallics in Al(Cu) alloy matrix composites by reaction sintering. *Materials Science and Engineering: A*. Vol. 380, No. 1–2, 2004, pp. 384–393.

[16] Dinaharan, I., M. Balakrishnan, J. David Raja Selvam, and E. T. Akinlabim. Microstructural characterization and tensile behavior of friction stir processed AA6061/Al_2Cu cast aluminum matrix composites. *Journal of Alloys and Compounds*. Vol. 781, 2019, pp. 270–279.

[17] Samal, P., R. V. Pandu, A. Meher, and M. M. Manas. Recent progress in aluminum metal matrix composites: A review on processing, mechanical and wear properties. *Journal of Manufacturing Processes*. Vol. 59, 2020, pp. 131–152.

[18] Rana, R. S., R. Purohit, and S. Das. Reviews on the influences of alloying elements on the microstructure and mechanical properties of aluminum alloys and aluminum alloy composites. *International Journal of Scientific Research*. Vol. 2, No. 6, 2012, pp. 1–7.

[19] Simões, S., F. Viana, M. A. L. Reis, and M. F. Vieira. Improved dispersion of carbon nanotubes in aluminum nanocomposites. *Composite Structures*. Vol. 108, 2014, pp. 992–1000.

[20] Chak, V., H. Chattopadhyay, and T. L. Dora. A review on fabrication methods, reinforcements and mechanical properties of aluminum matrix composites. *Journal of Manufacturing Processes*. Vol. 56, 2020, pp. 1059–1074.

[21] Senthil, S., M. Raguraman, and M. D. Thamarai. Manufacturing processes & recent applications of aluminium metal matrix composite materials: A review. *Materials Today: Proceedings*. Vol. 45, No. 7, 2021, pp. 5934–5938.

[22] C. Elanchezhian, R. M. Aravind, S. Annamalai, T. Atreya, V. Vignesh, C. Subramanian, et al. *Aluminium metal matrix composites - a review.* Reviews on Advanced Materials Science. Vol. 34, 2014, pp. 55–60.

[23] Ge, D. and M. Gu. Mechanical properties of hybrid reinforced aluminum based composites. *Materials Letters*. Vol. 49, No. 6, 2001, pp. 334–339.

[24] Zhang, W. X., L. X. Li, and T. J. Wang. Interface effect on the strengthening behavior of particle-reinforced metal matrix composites. *Computational Materials Science*. Vol. 41, No. 2, 2007, pp. 145–155.

[25] Lasagni, F. and H. P. Degischer. Enhanced Young's modulus of Al-Si alloys and reinforced matrices by Co-continuous

structures. *Journal of Composite Materials*. Vol. 44, No. 6, 2010, pp. 739–755.
[26] El-Mahallawi, I. S., A. Y. Shash, and A. E. Amer. Nanoreinforced cast Al-Si alloys with Al_2O_3, TiO_2 and ZrO_2 nanoparticles. *Metals*. Vol. 5, 2015, pp. 802–821.
[27] Hernandez-Sandoval, J., A. M. Samuel, F. H. Samuel, and S. Valtierra. Effect of additions of SiC and Al_2O_3 particulates on the microstructure and tensile properties of Al–Si–Cu–Mg cast alloys. *International Journal of Metalcasting*. Vol. 10, No. 3, 2016, pp. 253–263.
[28] Kang, H. G., M. Kida, H. Miyahara, and K. Ogi. Age hardening behaviour of alumina continuous fibre reinforced Al-Si-Cu and Al–Si–Cu–Mg alloys. *International Journal of Cast Metals Research*. Vol. 151, 2002, pp. 1–7.
[29] Xue, J., W. Wu, J. Ma, H. Huang, and Z. Zhao. Study on the effect of CeO_2 for fabricating *in-situ* TiB_2/A356 composites with improved mechanical properties. *Materials Science and Engineering: A*. Vol. 786, 2020, id. 139416.
[30] Oliveira, M., S. Agathopoulos, and J. M. F. Ferreira. The influence of Y_2O_3-containing sintering additives on the oxidation of Si_3N_4-based ceramics and the interfacial interactions with liquid Al-alloys. *Journal of the European Ceramic Society*. Vol. 25, No. 1, 2005, pp. 19–28.
[31] Karthikeyan, G., G. Elatharasan, S. Thulasi, and P. Vijayalakshmi. Tensile, compressive and heat transfer analysis of ZrO_2 reinforced aluminum LM6 alloy metal matrix composites. *Materials Today: Proceedings*. Vol. Vol 37, No. 2, 2021, pp. 303–309.
[32] Rakshath, S., B. Suresha, R. Kumar, and I. Saravanan. Dry sliding and abrasive wear behaviour of Al-7075 reinforced with alumina and boron nitride particulates. *Materials Today: Proceedings*. Vol. 22, No. 3, 2020, pp. 619–626.
[33] Frage, N., L. Levin, N. Frumin, M. Gelbstein, and M. P. Dariel. Manufacturing B_4C–(Al,Si) composite materials by metal alloy infiltration. *Journal of Materials Processing Technology*. Vol. 143, 2003, pp. 486–490.
[34] Dwivedi, S. P. Microstructure and mechanical behaviour of Al/B_4C metal matrix composite. *Materials Today: Proceedings*. Vol. 25, No. 4, 2020, pp. 751–754.
[35] Ibrahim, M. F., H. R. Ammar, A. M. Samuel, M. S. Soliman, and F. H. Samuel. On the impact toughness of Al-15 vol% B_4C metal matrix composites. *Composites Part B: Engineering*. Vol. 79, 2015, pp. 83–94.
[36] An, Q., X. Cong, P. Shen, and Q. Jiang. Roles of alloying elements in wetting of SiC by Al. *Journal of Alloys and Compounds*. Vol. 784, 2019, pp. 1212–1220.
[37] Li, X., H. Yan, Z. Wang, N. Li, J. Liu, and Q. Nie. Effect of heat treatment on the microstructure and mechanical properties of a composite made of Al–Si–Cu–Mg aluminum alloy reinforced with SiC particles. *Metals*. Vol. Vol 911, 2019, id. 1205.
[38] Lekatou, A., A. E. Karantzalis, A. Evangelou, V. Gousia, G. Kaptay, A. Gácsi, et al. Aluminium reinforced by WC and TiC nanoparticles (*ex-situ*) and aluminide particles (*in-situ*): Microstructure, wear and corrosion behaviour. *Materials and Design*. Vol. 65, 2015, pp. 1121–1135.
[39] Sharath Kumar, P. N., T. S. Sachit, N. Mohan, and M. AkshayPrasad. Dry sliding wear behaviour of Al –5Si-3Cu-0.5Mn alloy and its WC reinforced composites at elevated temperatures. *Materials Today: Proceedings*. Vol. 44, No. 1, 2021, pp. 566–572.
[40] He, C. N., N. Q. Zhao, C. S. Shi, and S. Z. Song. Fabrication of aluminum carbide nanowires by a nano-template reaction. *Carbon*. Vol. 484, 2010, pp. 931–938.
[41] Shreenivasaiah, P. H., T. Gowda, B. Kuldeep, K. P. Ravikumar, and K. P. Muthanna. Experimental investigation of cubic boron nitride reinforced Al2014 composites. *Materials Today: Proceedings*. Vol. 46, 2021, pp. 7760–7763.
[42] Fernández, H., S. Ordoñez, H. Pesenti, R. Espinoza González, and M. Leoni. Microstructure homogeneity of milled aluminum A356–Si_3N_4 metal matrix composite powders. *Journal of Materials Research and Technology*. Vol. 8, No. 3, 2019, pp. 2969–2977.
[43] Laha, T., S. Kuchibhatla, S. Seal, W. Li, and A. Agarwal. Interfacial phenomena in thermally sprayed multiwalled carbon nanotube reinforced aluminum nanocomposite. *Acta Materialia*. Vol. 55, No. 3, 2007, pp. 1059–1066.
[44] Noguchi, T., A. Magario, S. Fukazawa, S. Shimizu, J. Beppu, and M. Seki. Carbon Nanotube/Aluminium composites with uniform dispersion. *Materials Transactions*. Vol. 45, No. 2, 2004, pp. 602–604.
[45] Senthil Saravanan, M. S., S. P. Kumaresh Babu, and K. Sivaprasad. Mechanically alloyed carbon nanotubes (CNT) reinforced nanocrystalline AA 4032: synthesis and characterization. *Journal of Minerals and Materials Characterization and Engineering*. Vol. 911, 2010, pp. 1027–1035.
[46] Bakshi, S. R., A. K. Keshri, V. Singh, S. Seal, and A. Agarwal. Interface in carbon nanotube reinforced aluminum silicon composites: Thermodynamic analysis and experimental verification. *Journal of Alloys and Compounds*. Vol. 481, No. 1–2, pp. 207–213.
[47] Ahmad, S. I., H. Hamoudi, A. Abdala, Z. K. Ghouri, and K. M. Youssef. Graphene-reinforced bulk Metal Matrix Composites: Synthesis, microstructure, and properties. *Reviews on Advanced Materials Science*. Vol. 59, No. 1, 2020, pp. 67–114.
[48] Chen, W., T. Yang, L. Dong, A. Elmasry, J. Song, N. Deng, et al. Advances in graphene reinforced metal matrix nanocomposites: Mechanisms, processing, modelling, properties and applications editors-pick. *Nanotechnology and Precision Engineering*. Vol. 3, No. 4, 2020, pp. 189–210.
[49] Chak, V. and H. Chattopadhyay. Synthesis of graphene–aluminium matrix nanocomposites: mechanical and tribological properties. *Materials Science and Technology*. Vol. 37, No. 5, 2021, pp. 467–477.
[50] Chak, V. and H. Chattopadhyay. Fabrication and heat treatment of graphene nanoplatelets reinforced aluminium nanocomposites. *Materials Science and Engineering: A*. Vol. 791, 2020, id. 139657.
[51] Huang, Y., Q. Ouyang, D. Zhang, J. Zhu, R. Li, and H. Yu. Carbon Materials Reinforced Aluminum Composites: A Review. *Acta Metallurgica Sinica.* (*Eng. Lett.*). Vol. 27, No. 5, 2014, pp. 775–786.
[52] Dresch, A. B., J. Venturini, S. Arcaro, O. R. K. Montedo, and C. P. Bergmann. Ballistic ceramics and analysis of their mechanical properties for armour applications: A Review. *Ceramics International*. Vol. 47, No. 7, 2020, pp. 8743–8761.
[53] Peng, B., M. Locascio, P. Zapol, S. Li, S. L. Mielke, G. C. Schatz, et al. Measurements of near-ultimate strength for multiwalled carbon nanotubes and irradiation-induced crosslinking improvements. *Nature Nanotechnology*. Vol. 310, 2008, pp. 626–631.

[54] Orbulov, I. N. Metal matrix syntactic foams produced by pressure infiltration-The effect of infiltration parameters. *Materials Science and Engineering: A*. Vol. 583, 2013, pp. 11–19.
[55] Bolat., C., G. Bilge, and A. Gökşenli. An investigation on the effect of heat treatment on the compression behavior of aluminum matrix syntactic foam fabricated by sandwich infiltration casting. *Materials Research*. Vol. 24, No. 2, 2021, id. e20200381.
[56] Szlancsik, A., B. Katona, K. Májlinger, and I. N. Orbulov. Compressive behavior and microstructural characteristics of iron hollow sphere filled aluminum matrix syntactic foams. *Materials*. Vol. 811, 2015, pp. 7926–7937.
[57] Sazegaran, H., A. Kiani-Rashid, and J. V. Khaki. Effects of sphere size on the microstructure and mechanical properties of ductile iron–steel hollow sphere syntactic foams. *International Journal of Minerals, Metallurgy and Materials*. Vol. 23, 2016, pp. 676–682.
[58] Rabiei, A., L. Vendra, N. Reese, N. Young, and B. P. Neville. Processing and characterization of a new composite metal foam. *Materials Transactions*. Vol. 479, pp. 2148–2153.
[59] Rabiei, A. and L. J. Vendra. A comparison of composite metal foam's properties and other comparable metal foams. *Materials Letters*. Vol. 3, 2009, pp. 533–536.
[60] Chen, Z., Y. Zhang, J. Wang, H. GangaRao, R. Liang, Y. Zhang, et al. Experimental and modeling investigations of the behaviors of syntactic foam sandwich panels with lattice webs under crushing loads. *Reviews on Advanced Materials Science*. Vol. 60, No. 1, 2021, pp. 450–465.
[61] Luong, D. D., O. M. Strbik, V. H. Hammond, N. Gupta, and K. Cho. Development of high performance lightweight aluminum alloy/SiC hollow sphere syntactic foams and compressive characterization at quasi-static and high strain rates. *Journal of Alloys and Compounds*. Vol. 550, 2013, pp. 412–422.
[62] Guerrero, C. T., F. González, T. E. Soto, C. Aguilar, I. A. Figueroa, G. González, et al. An overview of the interactions between reinforcements and Al matrices with Si. Cu and Mg as alloying elements in aluminum matrix composites: case of oxide reinforcements. *Materials Research*. Vol. 25, 2022, id. e20210540.
[63] Fukunaga, H. *Aluminium metal matrix composites by reactive and semi-solid squeeze casting. In Metal and Ceramic Matrix Composites. Series in Materials Science and Engineering, Cantor*, B .F. Dunne and I. Stone, An Oxford–Kobe Materials Text, Institute of Physics Publishing, Bristol and Philadelphia, 2004, pp. 117–131. Chapter 8.
[64] Mavhungu, S. T., E. T. Akinlabi, M. A. Onitiri, and F. M. Varachia. Aluminum Matrix Composites for industrial use: Advances and trends. *Procedia Manufacturing*. Vol. 17, 2017, pp. 178–182.
[65] Moutinho Gomes, L. A. C., D. N. Travessa, J. L. González-Carrasco, M. Lieblich, and K. R. Cardoso. Production of MA956 alloy reinforced aluminum matrix composites by mechanical alloying. *Materials Research*. Vol. 18, 2015, pp. 48–54.
[66] Mitra, R. and Y. R. Mahajan. Interfaces in discontinuously reinforced metal matrix composites: An overview. *Bulletin of Materials Science*. Vol. 184, 1995, pp. 405–434.
[67] Wang, J., H. L. Duan, Z. Zhang, and Z. P. Huang. An anti-interpenetration model and connections between interphase and interface models in particle-reinforced composites. *International Journal of Mechanical Sciences*. Vol. 45, No. 4–5, 2005, pp. 701–718.
[68] Cayron, C. TEM study of interfacial reactions and precipitation mechanisms in Al_2O_3 short fiber or high volume fraction SiC particle reinforced Al-4Cu-1Mg-0.5Ag squeeze-cast composites. Thesis submitted to Swiss Federal Institute of Technology Lausanne (EPFL) for the degree of Doctor in Science. *CH-3602, Thun, March*, EMPA, 2001.
[69] Kaczmar, J. W., K. Naplocha, J., and Morgiel. . Microstructure and strength of Al_2O_3 and carbon fiber reinforced 2024 aluminum alloy composites. *Journal of Materials Engineering and Performance*. Vol. 23, No. 8, 2014, pp. 2801–2808.
[70] Feest, E. A. Interfacial phenomena in metal-matrix composites. *Composites*. Vol. 25, No. 2, 1994, pp. 75–86.
[71] Kandpal, B. C., J. Kumar, and H. Singh. Fabrication and characterisation of Al_2O_3/aluminium alloy 6061 composites fabricated by stir casting. *Materials Today: Proceedings*. Vol. 4, 2017, pp. 2783–2792.
[72] Baik, K. H., G. C. Lee, and S. Ahn. Interface and tensile behavior of squeeze cast AC8A- Al_2O_3 composite. *Scripta Metallurgica et Materialia*. Vol. 30, No. 2, 1994, pp. 235–239.
[73] Tekmen, C. and U. Cocen. The effect of Si and Mg on age hardening behavior of Al–SiCp composites. *Journal of Composite Materials*. Vol. 3720, 2003, pp. 1791–1800.
[74] Suryanarayanan, K. R. and S. R. Praveen. Silicon carbide reinforced aluminium metal matrix composites for aerospace applications: A Literature Review. *International Journal of Innovative Research in Science*. *Engineering and Technology*. Vol. 211, 2013, pp. 6336–6344.
[75] Neelima, D. C., V. Mahesh, and N. Selvaraj. Mechanical characterization of Aluminium silicon carbide composite. *International Journal of Applied Engineering Research*. Vol. 1, No. 4, 2011, pp. 793–799.
[76] Arsenault, R. The strengthening of aluminum alloy 6061 by fiber and platelet silicon carbide. *Materials Science and Engineering*. Vol. 64, No. 2, 1984, pp. 171–181.
[77] Dave, M. and K. Kothari. Composite Material-Aluminium Silicon Alloy: A Review. *Indian Journal of Research*. Vol. 2, No. 3, 2013, pp. 148–150.
[78] Rajan, T. P. D., R. M. Pillai, and B. C. Pai. Reinforcement coatings and interfaces in aluminium metal matrix composites. *Journal of Materials Science*. Vol. 3314, 1998, pp. 3491–3503.
[79] Iseki, T., T. Kameda, and T. Maruyama. Interfacial reactions between SiC and aluminium during joining. *Journal of Materials Science*. Vol. 19, No. 5, 1984, pp. 1692–1698.
[80] Chernyshova, T. and A. Rebrov. Interaction kinetics of boron carbide and silicon carbide with liquid aluminium. *Journal of the Less Common Metals*. Vol. 11712, 1986, pp. 203–207.
[81] Moshier, W., J. Ahearn, and D. Cooke. Interaction of Al-Si, Al-Ge, and Zn-Al eutectic alloys with SiC/Al discontinuously reinforced metal matrix composites. *Journal of Materials Science*. Vol. 22, No. 1, 1987, pp. 115–122.
[82] Salvo, L., G. L'Esperance, M. Suery, and J. G. Legoux. Interfacial reactions and age hardening in A1-Mg-Si metal matrix composites reinforced with SiC particles. *Materials Science and Engineering: A*. Vol. 177, 1994, pp. 173–183.

[83] Tham, L., M. Gupta, and L. Cheng. Effect of limited matrix–reinforcement interfacial reaction on enhancing the mechanical properties of aluminium–silicon carbide composites. *Acta Materialia*. Vol. 4916, 2001, pp. 3243–3253.

[84] Wang, A. Q., H. W. Tian, and J. P. Xie. Properties investigation and microstructures characterization of SiCp/6061Al composites produced by PM route. *IOP Conference Series Materials Science and Engineering*. Vol. 292, No. 1, 2018, id. 012055.

[85] Wang, Z., A. Wang, H. Han, and J. Xie. HRTEM study of interfacial structure in SiCp/A390 composites. *Materials Research Express*. Vol. 7, No. 4, 2020, id. 046514.

[86] Wang, D., B. L. Xiao, Q. Z. Wang, and Z. Y. Ma. Evolution of the microstructure and strength in the nugget zone of friction stir welded SiCp/Al–Cu–Mg composite. *Journal of Materials Science & Technology*. Vol. 30, No. 1, 2014, pp. 54–60.

[87] Luo, Z. P. Crystallography of SiC/$MgAl_2O_4$/Al interfaces in a pre-oxidized SiC reinforced SiC/Al composite. *Acta Materialia Volume*. Vol. 54, No. 1, 2006, pp. 47–58.

[88] Du, X., T. Gao, G. Liu, and X. Liu. *In situ* synthesizing SiC particles and its strengthening effect on an Al-Si-Cu-Ni-Mg piston alloy. *Journal of Alloys and Compounds*. Vol. 695, 2017, pp. 1–8.

[89] Sritharan, T., L. S. Chan, L. K. Tan, and N. P. Hung. A feature of the reaction between Al and SiC particles in an MMC. *Materials Characterization*. Vol. 47, No. 1, 2001, pp. 75–77.

[90] Park, J., J. Lee, I. Jo, S. Cho, S. K. Lee, S. B. Lee, et al. Surface modification effects of SiC tile on the wettability and interfacial bond strength of SiC tile/Al7075-SiCp hybrid composites. *Surface & Coatings Technology*. Vol. 307, 2016, pp. 399–406.

[91] Shi, Z. L., J. M. Yang, J. C. Lee, D. Zhang, H. I. Lee, and R. J. Wu. The interfacial characterization of oxidized SiC(p)/2014 Al composites. *Materials Science and Engineering: A*. Vol. 303, No. 1–2, 2001, pp. 46–53.

[92] Mogilevsky, R., S. R. Bryan, W. S. Wolbach, T. W. Krucek, R. D. Maier, G. L. Shoemaker, et al. Reactions at the matrix/reinforcement interface in aluminum alloy matrix composites. *Materials Science and Engineering: A*. Vol. 191, No. 1–2, 1995, pp. 209–222.

[93] Quigley, B. F., G. Abbaschian, R. Wunderlin, and R. Mehrabian. A method for fabrication of aluminium-alumina composites. *Metallurgical Transactions: A*. Vol. 13, No. 1, 1982, pp. 93–100.

[94] Hallstedt, B., Z. K. Liu, and J. Ågren. Fibre-matrix interactions during fabrication of Al_2O_3-Mg metal matrix composites. *Materials Science and Engineering: A*. Vol. 129, No. 1, 1990, pp. 135–145.

[95] Xie, B. and X. Wang. Thermo-physical properties and reaction process of SiCp/Al-7Si-5Mg Aluminum Matrix Composites fabricated by pressureless infiltration. *Rare Metal Materials and Engineering*. Vol. 44, No. 5, 2015, pp. 1057–1061.

[96] Li, J. G. Wetting of ceramic materials by liquid silicon, aluminium and metallic melts containing titanium and other reactive elements: A Review. *Ceramics International*. Vol. 20, 1994, pp. 391–412.

[97] Schwabe, U., L. R. Wolff, F. J. J. van Loo, and G. Ziegler. Corrosion of technical ceramics by molten aluminium. *Journal of the European Ceramic Society*. Vol. 9, No. 6, 1992, pp. 407–415.

[98] Ren, S., X. He, X. Qu, I. S. Humail, and Y. Li. Effect of Mg and Si in the aluminum on the thermo-mechanical properties of pressureless infiltrated SiCp/Al composites. *Composites Science and Technology*. Vol. 6710, 2007, pp. 2103–2113.

[99] Myriounis, D. P., S. T. Hasan, and T. E. Matikas. Microdeformation behaviour of Al–SiC metal matrix composites. *Composite Interfaces*. Vol. 15, No. 5, 2008, pp. 495–514.

[100] Mahendra, B. M., K. Arulshri, and N. Iyandurai. Evaluation of mechanical properties of aluminium alloy 2024 reinforced with silicon carbide and fly ash hybrid metal matrix composites. *American Journal of Applied Sciences*. Vol. 10, No. 4, 2013, pp. 219–229.

[101] Gonzalez, G., L. Salvo, M. Suéry, and G. L'Espérance. Interfacial reactions in Al-Mg metal matrix composites reinforced with (Sn/Sb) oxide coated SiC particles. *Scripta Metallugica et Materialia*. Vol. 3312, 1995, pp. 1969–1975.

[102] Li, B., B. Luo, K. He, L. Zeng, W. Fan, and Z. Bai. Effect of aging on interface characteristics of Al–Mg–Si/SiC composites. *Journal of Alloys and Compounds*. Vol. 64915, 2015, pp. 495–499.

[103] Henriksen, B. R., and I. Gionnes. Microstructure characterisation and mechanical properties of two SiC reinforced composites. *In Advanced structural inorganic composites*, P. Vincenzini, Ed, Elsevier Science Publishers, Amsterdam, 1991, pp. 251–258.

[104] Lucas, I. P., N. Y. C. Yang, I. I. Stephens. Interface and near-interface microstructure of discontinuous reinforced metal matrix composites. In MRS structure and properties of interfaces in materials. *Materials Research Society Proceedings of Symposium*, W. A. T. Clark, U. Dahmen, C. L. Briant, Eds, 1992, pp. 877–883. Pittsburgh, PA.

[105] Manor, E., H. Ni, and C. G. Levi. Microstructure evolution of SiC/Al_2O_3/Al-Alloy composites produced by melt oxidation. *Journal of the American Ceramic Society*. Vol. 76, No. 7, 1993, pp. 1777–1787.

[106] Sritharan, T., K. Xia, J. Heathcock, and J. Mihelich. Matrix/reinforcement development for aluminium-based composites. In *Metal and ceramic matrix composites: processing, modelling and mechanical behavior*, R. B. Bhagat, A. H. Clauer, P. Kumar, and A. M. Ritter, Eds, TMS, Warrendale, PA, 1990, pp. 13–22.

[107] Gao, Y. Y., F. Qiu, R. Geng, W. X. Zhao, D. L. Yang, R. Zuo, et al. Preparation and characterization of the Al-Cu-Mg-Si-Mn composites reinforced by different surface modified SiCp. *Materials Characterization*. Vol. 141, 2018, pp. 156–162.

[108] Sukumaran, K., S. Pillai, R. Pillai, V. Kelukutty, B. Pai, K. Satyanarayana, et al. The effects of magnesium additions on the structure and properties of Al-7Si-10SiC composites. *Journal of Materials Science*. Vol. 30, No. 6, 1995, pp. 1469–147.

[109] Feng, Y., J. P. Ren, C. G. Dong, C. Peng, and R. Wang. Microstructures and properties of the copper-coated SiCp Reinforced Al–Si alloy composites. *Advance Engineering Materials*. Vol. 19, No. 6, 2017, id. 1600816.

[110] Pal, S., R. Mitra, and V. V. Bhanuprasad. Aging behaviour of Al–Cu–Mg alloy–SiC composites. *Materials Science and Engineering: A*. Vol. 480, 2008, pp. 496–505.

[111] Durbadal, M. and V. Srinath. Effect of re-melting on particle distribution and interface formation in SiC reinforced 2124 Al

matrix composite. *Materials Characterization*. Vol. 86, 2013, pp. 21–27.
[112] Song, Y. F., X. F. Ding, X. J. Zhao, L. R. Xiao, and C. X. Yu. The effect of SiC addition on the dimensional stability of Al-Cu-Mg alloy. *Journal of Alloys and Compounds*. Vol. 750, 2018, pp. 111–116.
[113] Gatea, S., H. Ou, and G. McCartney. Deformation and fracture characteristics of Al6092/SiC/17.5p metal matrix composite sheets due to heat treatments. *Materials Characterization*. Vol. 142, 2018, pp. 365–376.
[114] Guo, X., Q. Guo, J. Nie, Z. Liu, Z. Li, G. Fan, et al. Particle size effect on the interfacial properties of SiC particle-reinforced Al-Cu-Mg composites. *Materials Science and Engineering: A*. Vol. 711, 2018, pp. 643–649.
[115] Varma, V. K., Y. R. Mahajan, and V. V. Kutumbarao. Ageing behaviour of Al-Cu-Mg alloy matrix composites with SiC of varying sizes. *Scripta Materialia*. Vol. 37, No. 4, 1997, pp. 485–489.
[116] Zhang, Q., B. L. Xiao, Z. Y. Liu, and Z. Y. Ma. Microstructure evolution and elemental diffusion of SiCp/Al–Cu–Mg composites prepared from elemental powder during hot pressing. *Journal of Materials Science*. Vol. 4621, 2011, pp. 6783–6793.
[117] Wang, T., M. Yamamoto, and A. Kagawa. Influence of interfacial reaction on wear resistance of aluminum alloy/SiC composites fabricated by low pressure infiltration process. *Materials Transactions*. Vol. 56, No. 7, 2015, pp. 1081–1086.
[118] Wu, Y. Y., X. F. Liu, G. L. Ma, C. Li, and J. Zhang. High energy milling method to prepare Al/WC composite coatings in Al-Si alloys. *Journal of Alloys and Compounds*. Vol. 497, No. 1, 2010, pp. 139–41.
[119] Lou, D., J. Hellman, D. Luhulima, J. Liimatainen, and V. K. Lindroos. Interactions between tungsten carbide (WC) particulates and metal matrix in WC-reinforced composites. *Materials Science & Engineering: A*. Vol. 340, No. 1–2, 2003, pp. 155–162.
[120] Anwer, A. H. Effect of the reinforcing by WC on microhardness, roughness and corrosion behavior of Al-12Si alloy. *Engineering and Technology Journal*. Vol. 3415, 2016, pp. 2891–2896.
[121] Krishna, U. B. G., P. Ranganatha, G. L. Rajesh, V. Auradi, S. Kumar, B. Mahendra, et al. Studies on dry sliding wear characteristics of cermet WC-Co particulate reinforced Al7075 metal matrix composite. *Materials Today: Proceedings*. Vol. 16, No. 2, 2019, pp. 343–350.
[122] Zhang, H., P. Feng, and F. Akhtar. Aluminium matrix tungsten aluminide and tungsten reinforced composites by solid-state diffusion mechanism. *Scientific Reports*. Vol. 7, 2017, id. 12391.
[123] Li, F., Z. Gao, Y. Zhang, and Y. Chen. Alloying effect of titanium on WCp/Al composite fabricated by coincident wire-powder laser deposition. *Materials & Design*. Vol. 93, 2016, pp. 370–378.
[124] Huang, G., W. Hou, and Y. Shen. Evaluation of the microstructure and mechanical properties of WC particle reinforced aluminum matrix composites fabricated by friction stir processing. *Materials Characterization*. Vol. 138, 2018, pp. 26–37.
[125] Rodríguez-Cabriales, G., A. M. Lometo-Sánchez, J. C. Guía-Tello, H. M. Medrano-Prieto, E. J. Gutiérrez-Castañeda, I. Estrada-Guel, et al. Synthesis and characterization of Al-Cu-Mg system reinforced with tungsten carbide through powder metallurgy. *Materials Today Communications*. Vol. 22, 2020, id. 100758.
[126] Chao, Z. L., L. C. Zhang, L. T. Jiang, J. Qiao, Z. G. Xu, H. T. Chi, et al. Design, microstructure and high temperature properties of *in-situ* Al_3Ti and nano-Al_2O_3 reinforced 2024Al matrix composites from Al-TiO_2 system. *Journal of Alloys and Compounds*. Vol. 775, 2019, pp. 290–297.
[127] Singh, G. and N. Sharma. Study on the influence of T4 and T6 heat treatment on the wear behavior of coarse and fine WC particulate reinforced LM28 Aluminium cast composites. *Composites Part C: Open Access*. Vol. 4, 2021, id. 100106.
[128] Liu, C. Y., Q. Wang, Y. Z. Jia, B. Zhang, R. Jing, M. Z. Ma, et al. Evaluation of mechanical properties of 1060-Al reinforced with WC particles via warm accumulative roll bonding process. *Materials and Design*. Vol. 43, 2013, pp. 367–372.
[129] Prasad, D. S., P. T. Radha, C. Shoba, and P. S. Rao. Dynamic mechanical behavior of WC-Co coated A356.2 aluminum alloy. *Journal of Alloys and Compounds*. Vol. 767, 2018, pp. 988–993.
[130] Staia, M. H., M. Cruz, and N. B. Dahotre. Microstructural and tribological characterization of an A-356 aluminum alloy superficially modified by laser alloying. *Thin Solid Films*. Vol. 377–378, 2000, pp. 665–674.
[131] Katkar, V. A., G. Gunasekaran, A. G. Rao, and P. M. Koli. Effect of the reinforced boron carbide particulate content of AA6061 alloy on formation of the passive film in seawater. *Corrosion Science*. Vol. 53, No. 9, 2011, pp. 2700–2712.
[132] Oh, S. Y., J. A. Cornie, and K. C. Russel. Wetting of ceramic particulates with liquid aluminium alloys. Part II. Study of wettability. *Metallurgical Transactions: A*. Vol. 20, 1989, pp. 533–541.
[133] Jung, J. and S. Kang. Advances in manufacturing boron carbide-aluminum composites. *Journal of the American Ceramic Society*. Vol. 87, No. 1, 2004, pp. 47–54.
[134] Auradi, V., G. L. Rajesh, and S. A. Kori. Processing of B_4C particulate reinforced 6061aluminum matrix composites by melt stirring involving two-step addition. *Procedia Materials Science*. Vol. 6, 2014, pp. 1068–1076.
[135] Canakci, A., A. Fazil, and Y. Ibrahim. Pre-treatment process of B_4C particles to improve incorporation into molten AA2014 alloy. *Journal of Materials Science*. Vol. 42, 2017, pp. 9536–9542.
[136] Toptan, F., A. Kilicarslan, A. Karaaslan, M. Cigdem, and I. Kerti. Processing and microstructural characterisation of AA 1070 and AA 6063 matrix B_4Cp reinforced composites. *Materials and Design*. Vol. 31, 2010, pp. S87–S91.
[137] Chellapandi, P., A. S. Kumar, and S. Vendan. Arungalai. Experimental investigations on aluminum based metal matrix composites with B_4C, SiC and Mg. *Carbon - Science and Technology*. Vol. 7, No. 1, 2015, pp. 59–68.
[138] Lestari, A. D. D. and A. Z. Syahrial. The characteristics of aluminum AC_4B composites reinforced by the fraction volume variations of Boron Carbide through the stir casting process. *IOP Conference Series. Materials Science and Engineering*. Vol. 673, 2019, id. 012134.
[139] Zhang, Z., K. Fortin, A. Charette, and X. G. Chen. Fluidity and microstructure evolution of Al-12%B_4C composites

containing magnesium. *Materials Transactions*. Vol. 52, No. 5, 2011, pp. 928–933.
[140] Zhou, Y., Y. Zan, S. Zheng, X. Shao, Q. Jin, B. Zhang, et al. Thermally stable microstructures and composite mechanical properties of B_4C-Al with *in-situ* formed Mg(Al) B_2. *Journal of Materials Science and Technology*. Vol. 35, 2019, id. 1830.
[141] Viala, J. C., P. Foretier, and J. Bouix. Stable and metastable phase equilibria in the chemical interaction between aluminium and silicon carbide. *Journal of Materials Science*. Vol. 25, 1990, pp. 1842–1850.
[142] Lucas, J. P., J. J. Stephens, and F. A. Greulich. The effect of reinforcement stability on composition redistribution in cast aluminum metal matrix composites. *Materials Science and Engineering: A*. Vol. 131, No. 2, 1991, pp. 221–230.
[143] Pyzic, A. J. and D. R. Beaman. Al-B-C phase development and effects on mechanical properties of B_4C/Al-derived composites. *Journal of the American Ceramic Society*. Vol. 78, No. 2, 1995, pp. 305–312.
[144] Lee, D., J. Kim, S. K. Lee, Y. Kim, S. B. Lee, and S. Cho. Experimental and thermodynamic study on interfacial reaction of B_4C–Al6061 composites fabricated by stir casting process. *Journal of Alloys and Compounds*. Vol. 859, 2021, id. 157813.
[145] Lee, K. B., H. S. Sim, S. Y. Cho, and H. Kwon. Reaction products of Al-Mg/B_4C composite fabricated by pressureless infiltration technique. *Materials Science and Engineering: A*. Vol. 302, No. 2, 2001, pp. 227–234.
[146] Lee, K. B., Y. S. Kim, and H. Kwon. Fabrication of Al-3 Wt pct Mg matrix composites reinforced with Al_2O_3 and SiC particulates by the pressureless infiltration technique. *Metallurgical and Materials Transactions: A*. Vol. 2912, 1998, pp. 3087–3095.
[147] Lee, K. B. and H. Kwon. Fabrication and characteristics of AA6061/Si_3N_{4p} composite by the pressureless infiltration technique. *Metallurgical and Materials Transactions: A*. Vol. 3011, 1999, pp. 2999–3007.
[148] Shamekh, M., M. Pugh, and M. Medraj. Understanding the reaction mechanism of *in-situ* synthesized ($TiCeTiB_2$)/AZ91 magnesium matrix composites. *Materials Chemistry and Physics*. Vol. 135, No. 1, 2012, pp. 193–205.
[149] Suárez, O. M., J. Vazquez, and L. Reyes-Russi. Synthesis and characterization of mechanically alloyed Al/AlxMg1-xB2 composites. *Science and Engineering of Composite Materials*. Vol. 16, No. 4, 2009, pp. 267–276.
[150] Li, Y. Z., Q. Z. Wang, W. G. Wang, B. Xiao, and Z. Y. Ma. Interfacial reaction mechanism between matrix and reinforcement in B_4C/6061Al composites. *Materials Chemistry and Physics*. Vol. 154, 2015, pp. 107–117.
[151] Xue, W., L. Jiang, B. Zhang, D. Jing, T. He, G. Chen, et al. Quantitative analysis of the effects of particle content and aging temperature on aging behavior in B_4C/6061Al composites. *Materials Characterization*. Vol. 163, 2020, id. 110305.
[152] Zhou, Y. T., Y. N. Zan, S. J. Zheng, Q. Z. Wang, B. L. Xiao, X. L. Ma, et al. Distribution of the microalloying element Cu in B_4C-reinforced 6061Al Composites. *Journal of Alloys and Compounds*. Vol. 728, 2017, pp. 112–117.
[153] Pozdniakov, A. V., A. Lotfy, A. Qadir, E. Shalaby, M. G. Khomutov, A. Y. Churyumov, et al. Development of Al-5Cu/B_4C composites with low coefficient of thermal expansion for automotive application. *Materials Science and Engineering: A*. Vol. 688, 2017, pp. 1–8.
[154] Manning, Jr. C. R., and T. B. Gurganus. Wetting of binary aluminum alloys in contact with Be, B_4C, and Graphite. *Journal of the American Ceramic Society*. Vol. Vol 52, No. 3, 1969, pp. 115–118.
[155] Kuang, W., B. Zhao, C. Yang, and W. Ding. Effects of h-BN particles on the microstructure and tribological property of self-lubrication CBN abrasive composites. *Ceramics International*. Vol. 46, No. 2, 2020, pp. 2457–2464.
[156] Chen, C., L. Guo, J. Luo, J. Hao, Z. Guo, and A. A. Volinsky. Aluminum powder size and microstructure effects on properties of boron nitride reinforced aluminum matrix composites fabricated by semi-solid powder metallurgy. *Materials Science and Engineering: A*. Vol. 646, 2015, pp. 306–314.
[157] Lotfy, A., A. V. Pozdniakov, V. S. Zolotorevskiy, M. T. Abou Elkhair, A. Daoud, and A. G. Mochugovskiy. Novel preparation of Al-5%Cu/BN and Si_3N_4 composites with analyzing microstructure, thermal and mechanical properties. *Materials Characterization*. Vol. 136, 2018, pp. 144–151.
[158] Duan, X., Z. Yang, L. Chen, Z. Tian, D. Cai, Y. Wang, et al. Review on the properties of hexagonal boron nitride matrix composite ceramics. *Journal of the European Ceramic Society*. Vol. 3615, 2016, pp. 3725–3737.
[159] Fujii, H., H. Nakae, and K. Okada. Interfacial reaction wetting in the boron nitride/molten aluminum system. *Acta Metallurgica et Materialia*. Vol. 4110, 1993, pp. 2963–2971.
[160] Lee, K. B., H. S. Sim, S. W. Heo, H. R. Yoo, S. Y. Cho, and H. Kwon. Tensile properties and microstructures of Al composite reinforced with BN particles. *Composites: Part A*. Vol. 33, No. 5, 2002, pp. 709–715.
[161] Khatavkar, R. A., A. K. Mandave, D. D. Baviskar, and S. L. Shinde. Influence of hexagonal boron nitride on tribological properties of AA2024-hBN Metal Matrix Composite. *International Research Journal of Engineering and Technology*. Vol. 5, No. 5, 2018, pp. 3792–3798.
[162] Woo, W. S., W. G. Jung, and D. B. Lee. Oxidation behavior of BN/(Al-Mg) Metal Matrix Composites. *Materials Science Forum*. Vol. 475–479, 2005, pp. 975–978.
[163] Konopatsky, A. S., D. G. Kvashnin, S. Corthay, I. Boyarintsev, K. L. Firestein, A. Orekhov, et al. Microstructure evolution during AlSi10Mg molten alloy/BN microflake interactions in metal matrix composites obtained through 3D printing. *Journal of Alloys and Compounds*. Vol. 859, 2021, id. 157765.
[164] Ye, F., J. Y. Zhang, L. M. Liu, and H. J. Zhan. Effect of solid content on pore structure and mechanical properties of porous silicon nitride ceramics produced by freeze casting. *Materials Science and Engineering: A*. Vol. 528, 2011, pp. 1421–1424.
[165] Iwasaki, H., M. Mabuchi, K. Higashi, and T. G. Langdon. The development of cavitation in superplastic aluminum composite reinforced with Si_3N_4. *Materials Science and Engineering: A*. Vol. 208, 1996, pp. 116–121.
[166] Lu, Y., J. Yang, W. Lu, R. Liu, G. Qiao, and C. Bao. The mechanical properties of co-continuous Si_3N_4/Al composites manufactured by squeeze casting. *Materials Science and Engineering: A*. Vol. 52723, 2010, pp. 6289–6299.
[167] Akhtar, F. and S. Guo. Development of Si_3N_4/A1 composite by pressureless melt infiltration. *Transactions of Nonferrous Metals Society of China*. Vol. 16, 2006, pp. 629–632.

[168] De la Peña, J. L. and M. I. Pech-Canul. Reactive wetting and spreading of Al–Si–Mg alloys on Si_3N_4/Si substrates. *Materials Science and Engineering: A*. Vol. 491, No. 1–2, 2008, pp. 461–469.
[169] Koike, J., M. Mabuchi, and K. Higashi. Partial melting and segregation behavior in a superplastic Si_3N_4/Al-Mg alloy composite. *Journal of Materials Research*. Vol. 10, No. 1, 1995, pp. 133–138.
[170] Wang, S., Y. Wang, Y. Wang, H. Geng, and Q. Chi. Microstructure and infiltration kinetics of Si_3N_4/Al–Mg composites fabricated by pressureless infiltration. *Journal of Materials Science*. Vol. 42, 2007, pp. 7812–7818.
[171] Qu, S., A. Feng, L. Geng, J. Shen, and D. Chen. Silicon nitride whisker-reinforced aluminum matrix composites: twinning and precipitation behavior. *Metals*. Vol. 10, No. 3, 2020, id. 420.
[172] Yang, W., Z. Xiu, G. Chen, and G. Wu. Microstructure and thermal conductivity of submicron Si_3N_4 reinforced 2024Al composite. *Transactions of Nonferrous Metals Society of China*. Vol. 192, 2009, pp. s378–s381.
[173] Jeong, H. G., K. Hiraga, M. Mabuchi, and K. Higashi. Effects of addition of magnesium on interface structure and high-strain-rate superplasticity in Si_3N_4-reinforced al-alloy composites. *Acta Materialia*. Vol. 4617, 1998, pp. 6009–6020.
[174] Feng, A. H., L. Geng, J. Zhang, and C. K. Yao. Hot compressive deformation behavior of a eutectic Al–Si alloy based composite reinforced with α-Si_3N_4 whisker. *Materials Chemistry and Physics*. Vol. 82, No. 2, 2003, pp. 618–621.
[175] Chen, G., W. Yang, K. Ma, H. Murid, L. Jiang, and W. Wu. Aging and thermal expansion behavior of Si_3N_4p/2024Al composite fabricated by pressure infiltration method. *Transactions of Nonferrous Metals Society of China*. Vol. 21, No. Suppl. 2, 2011, pp. s262–s273.
[176] Banhart, F. Interactions between metals and carbon nanotubes: at the interface between old and new materials. *Nanoscale*. Vol. 1, No. 2, 2009, pp. 201–213.
[177] Reddy, B. M. and P. Anand. Exploration of properties of Al 5056/CNT metal matrix nano composites. *Materials Today: Proceedings*. Vol. 18, No. 7, 2019, pp. 4360–4365.
[178] Abbasipour, B., B. Niroumand, S. M. M. Vaghefi, and M. Abedi. Tribological behavior of A356–CNT nanocomposites fabricated by various casting techniques. *Transactions of Nonferrous Metals Society of China*. Vol. 2910, 2019, pp. 1993–2004.
[179] Yu, N. and Y. W. Chang. Effects of CNT diameter on the uniaxial stress-strain behavior of CNT/Epoxy composites. *Journal of Nanomaterials*. Vol. 2008, 2008, id. 834248.
[180] Park, S. H. and P. R. Bandaru. Improved mechanical properties of carbon nanotube/polymer composites through the use of carboxyl-epoxide functional group linkages. *Polymer*. Vol. 5122, 2010, pp. 5071–5077.
[181] Wu, Y. and G. Y. Kim. Carbon nanotube reinforced aluminum composite fabricated by semi-solid powder processing. *Journal of Materials Processing Technology*. Vol. 211, No. 8, 2011, pp. 1341–1347.
[182] Ci, L., Z. Ryu, N. Y. Jin-Phillipp, and M. Rühle. Investigation of the interfacial reaction between multi-walled carbon nanotubes and aluminum. *Acta Materialia*. Vol. 54, No. 20, 2006, pp. 5367–5375.
[183] Zhou, W., S. Bang, H. Kurita, T. Miyazaki, Y. Fan, and A. Kawasaki. Interface and interfacial reactions in multi-walled carbon nanotube-reinforced aluminum matrix composites. *Carbon*. Vol. 96, 2016, pp. 919–928.
[184] Landry, K., S. Kalogeropoulou, and N. Eustathopoulos. Wettability of carbon by aluminum and aluminum alloys. *Materials Science and Engineering: A*. Vol. 254, No. 1–2, 1998, pp. 99–111.
[185] Kwon, H., M. Estili, K. Takagi, T. Miyazaki, and A. Kawasaki. Combination of hot extrusion and spark plasma sintering for producing carbon nanotube reinforced aluminum matrix composites. *Carbon*. Vol. 47, No. 3, 2009, pp. 570–577.
[186] Bakshi, S. R. and A. Agarwal. An analysis of the factors affecting strengthening in carbon nanotube reinforced aluminum composites. *Carbon*. Vol. 49, No. 2, 2011, pp. 533–544.
[187] Abbasipour, B., B. Niroumand, and S. M. M. Vaghefi. Compocasting of A356-CNT composite. *Transactions of Nonferrous Metals Society of China*. Vol. 20, No. 9, 2010, pp. 1561–1566.
[188] Elshalakany, A. B., T. Osman, A. Khattab, B. Azzam, and M. Zaki. Microstructure and mechanical properties of MWCNTs reinforced A356 aluminum alloys cast nanocomposites fabricated by using a combination of rheocasting and squeeze casting techniques. *Journal of Nanomaterials*. Vol. 2014, 2014, id. 386370.
[189] Deng, C. F., X. X. Zhang, D. Z. Wang, and Y. X. Ma. Calorimetric study of carbon nanotubes and aluminum. *Materials Letters*. Vol. 6114, 2007, pp. 3221–3223.
[190] Kondoh, K., H. Fukuda, J. Umeda, H. Imai, and B. Fugetsu. Microstructural and mechanical behavior of multi-walled carbon nanotubes reinforced Al–Mg–Si alloy composites in aging treatment. *Carbon*. Vol. 72, 2014, pp. 15–21.
[191] Nam, D. H., Y. K. Kim, S. I. Cha, and S. H. Hong. Effect of CNTs on precipitation hardening behavior of CNT/Al-Cu composites. *Carbon*. Vol. 5013, 2012, pp. 4809–4814.
[192] Choi, H. J., B. H. Min, J. H. Shin, and D. H. Bae. Strengthening in nanostructured 2024 aluminum alloy and its composites containing carbon nanotubes. *Composites Part A*. Vol. 42, No. 10, 2011, pp. 1438–1844.
[193] Meng, X., T. Liu, C. Shi, E. Liu, C. N. He, and N. Q. Zhao. Synergistic effect of CNTs reinforcement and precipitation hardening in *in-situ* CNTs/Al–Cu composites. *Materials Science and Engineering: A*. Vol. 633, 2015, pp. 103–111.
[194] Fukuda, H., K. Kondoh, J. Umeda, and B. Fugetsu. Aging behavior of the matrix of aluminum-magnesium-silicon alloy including carbon nanotubes. *Materials Letters*. Vol. 65, 2011, pp. 1723–1725.
[195] Jagannatham, M., P. Chandran, S. Sankaran, P. Haridoss, N. Nayan, and S. R. Bakshi. *Tensile properties of carbon nanotubes reinforced aluminum matrix composites: A review*. Carbon. Vol. 160, 2020, pp. 14–44.
[196] Liu, Z., G. Zu, H. Luo, Y. Liu, and G. Yao. Influence of Mg Addition on graphite particle distribution in the Al Alloy Matrix Composites. *Journal of Materials Science and Technology*. Vol. 26, No. 3, 2010, pp. 244–250.
[197] Pelleg, J., D. Ashkenazi, and M. Ganor. The influence of a third element on the interface reactions in metal–matrix composites (MMC): Al–graphite system. *Materials Science and Engineering: A*. Vol. 281, No. 3, 2000, pp. 239–247.

[198] Shahverdi, H. R., M. R. Ghomashchi, S. Shabeatari, and J. Hejazi. Kinetics of interfacial reaction between solid iron and molten aluminium. *Journal of Materials Science*. Vol. 37, No. 5, 2002, pp. 1061–1066.
[199] Lee, I. S., P. W. Kao, and N. J. Ho. Microstructure and mechanical properties of Al–Fe *in situ* nanocomposite produced by friction stir processing. *Intermetallics*. Vol. 16, No. 9, 2008, pp. 1104–1108.
[200] Bouche, K., F. Barbier, and A. Coulet. Intermetallic compound layer growth between solid iron and molten aluminium. *Materials Science and Engineering: A*. Vol. 249, No. 1–2, 1998, pp. 167–175.
[201] Maitra, T. and S. P. Gupta. Intermetallic compound formation in Fe–Al–Si ternary system: Part II. *Materials Characterization*. Vol. 49, No. 4, 2002, pp. 293–311.
[202] Guo, Z., M. Liu, X. Bian, M. Liu, and J. Li. An Al–7Si alloy/cast iron bimetallic composite with super-high shear strength. *Journal of Materials Research and Technology*. Vol. 8, No. 3, 2019, pp. 3126–3136.
[203] Vendra, L. J. and A. Rabiei. A study on aluminum–steel composite metal foam processed by casting. *Materials Science and Engineering: A*. Vol. 465, No. 1–2, 2007, pp. 59–67.
[204] Garcia-Avila, M. and A. Rabiei. Effect of sphere properties on microstructure and mechanical performance of cast composite metal foams. *Metals*. Vol. 5, No. 2, 2015, pp. 822–835.
[205] Ghosh, G. A Comprehensive compendium of evaluated constitutional data and phase diagrams. *Aluminium–Iron–Silicon*, Vol. 5, 1a ed. G. Petzow, and G. Effenberg, Eds, VCH, Weinheim (Federal Republic of Germany), 1992, p. 695.
[206] Bálint, A. and A. Szlancsik. Mechanical properties of iron hollow sphere reinforced metal matrix syntactic foams. *Materials Science Forum*. Vol. 812, 2015, pp. 3–8.
[207] Orbulov, I. N. and J. Ginsztler. Compressive characteristics of metal matrix syntactic foams. *Composites Part A: Applied Science and Manufacturing*. Vol. 43, No. 4, 2012, pp. 553–561.
[208] Vendra, L. and A. Rabiei. Evaluation of modulus of elasticity of composite metal foams by experimental and numerical techniques. *Materials Science and Engineering: A*. Vol. 527, No. 7–8, 2010, pp. 1784–1790.